REPORT 935

TWO-DIMENSIONAL COMPRESSIBLE FLOW IN TURBOMACHINES WITH CONIC FLOW SURFACES

By John D. Stanitz

SUMMARY

A general method of analysis is developed for two-dimensional, steady, compressible flow in stators or rotors of radial- and mixed-flow turbomachines with conic flow surfaces (surfaces of right circular cones generated by center line of flow passage in the axial-radial plane). The variables taken into account are: (1) tip speed of the rotor, (2) flow rate, (3) blade shape, (4) variation in passage height with radius, (5) number of blades, and (6) cone angle of the flow surface. Relaxation methods are used to solve the nonlinear differential equation for the stream function.

The analysis indicates that: (1) The solution obtained for a given turbomachine also applies to certain other (equivalent) turbomachines with a larger or smaller number of like passages (same spacing of the blades on the conic flow surface, same blade-thickness distribution, and so forth) but with different cone angles; (2) for the same number of similar blades, the blade loading is less for mixed-flow than for radial-flow turbomachines; and (3) any solution obtained for an outflow turbomachine with shockless (smooth) entry is also the solution for an inflow turbomachine with shockless entry and with the flow direction and blade rotation (if any) reversed.

Two numerical examples are presented; one for compressible and the other for incompressible flow in a centrifugal compressor with thin, straight blades. The solutions were obtained in a region of the compressor, including the impeller tip, that was assumed to be unaffected by the inlet configuration of the impeller or by the diffuser vanes (if any). Both examples are for the same impeller (18° included angle between blades on conic flow surface) with the same tip speed (equivalent to a tip Mach number of 1.5 for the compressible-flow example), with the same flow rate, and with a constant flow area normal to the flow surface. The results of these examples are given by plots of the streamlines, constant velocity-ratio lines, and constant pressure-ratio lines.

It is concluded from the examples that, if the fluid in high-speed, rotating, radial- and mixed-flow blade systems is compressible, incompressible solutions give poor quantitative results (exception, the slip factor) and, in some respects, poor qualitative results.

INTRODUCTION

Increased knowledge of flow conditions within radial- and mixed-flow compressors and turbines should indicate means of improving performance of these turbomachines. For example, boundary-layer separation, which decreases the efficiency of these machines, can be minimized or eliminated by aerodynamic design based on knowledge of the velocity gradients that result from various design configurations.

For a given set of operating conditions, the flow conditions within radial- and mixed-flow turbomachines depend on the geometry of the machine (three-dimensional-flow effects) and on the properties of the fluid (compressibility and viscosity). Most treatments of the problem have been concerned with the two-dimensional-flow effects for incompressible, nonviscous fluids. (For example, see references 1 to 5.)

In the analysis reported herein, compressibility is considered. This consideration is especially important in radial- and mixed-flow turbomachines because the large pressure ratios per stage result in density changes that greatly affect the fluid velocities, and so forth. The analysis is developed for two-dimensional, compressible, nonviscous, steady flow through stators or rotors of radial- and mixed-flow turbomachines in which the center line of the flow passage in the axial-radial plane generates the surface of a right circular cone when rotated about the axis of the machine. The two-dimensional-flow pattern is considered to lie upon this surface.

The solution of two-dimensional, compressible-flow equations can be accomplished by relaxation methods, which were developed by Southwell (references 6 and 7) and which have been applied to compressible-flow problems by Emmons (reference 8). It is essentially the procedure outlined in reference 8 that is employed in the numerical solution of the differential equation obtained in this analysis.

The analysis is developed for turbomachines with arbitrary blade shapes and is applied, in the numerical examples, to a flow region, including the impeller tip, of a centrifugal compressor with straight, thin blades that lie on conic radii (elements). A simplified analysis for straight blades lying on conic radii is developed that checks the results of the relaxation solution within the impeller except for the flow region near the impeller tip.

This analysis was developed at the NACA Cleveland laboratory in 1947.

ANALYSIS

PRELIMINARY CONSIDERATIONS

This analysis develops a general method whereby the streamlines, velocity distribution, and pressure distribution can be determined for steady, two-dimensional compressible flow in stators or rotors of radial- and mixed-flow turbomachines with arbitrary blade shapes and varying passage

heights. The radial component of the flow may be in the direction of increasing radius (outflow turbomachine) or in the direction of decreasing radius (inflow turbomachine).

Conic flow surface.—The analysis is limited to turbomachines in which the center line of the passage in the axial-radial plane generates the surface of a right circular cone, with the cone angle α (fig. 1), when rotated about the axis of the machine. (All symbols are defined in appendix A.) The two-dimensional-flow pattern is considered to lie upon this cone surface (hereinafter referred to as "conic flow surface"). For mixed-flow turbomachines the cone angle α is less than 180° but greater than 0°. For the special case in which α is 180°, the conic flow surface becomes flat and is normal to the axis of the machine. Such turbomachines (α=180°) are designated radial-flow machines. For the special case in which α is 0°, the conic flow surface becomes cylindrical and is concentric with the axis of the machine. Such turbomachines (α=0°) are designated axial-flow machines. Axial-flow machines are not considered in this analysis for reasons that are subsequently discussed.

Coordinate system.—The developed view of a conic flow surface is shown in figure 2. The dimensionless, conic coordinates R and θ of this conic flow surface are relative to

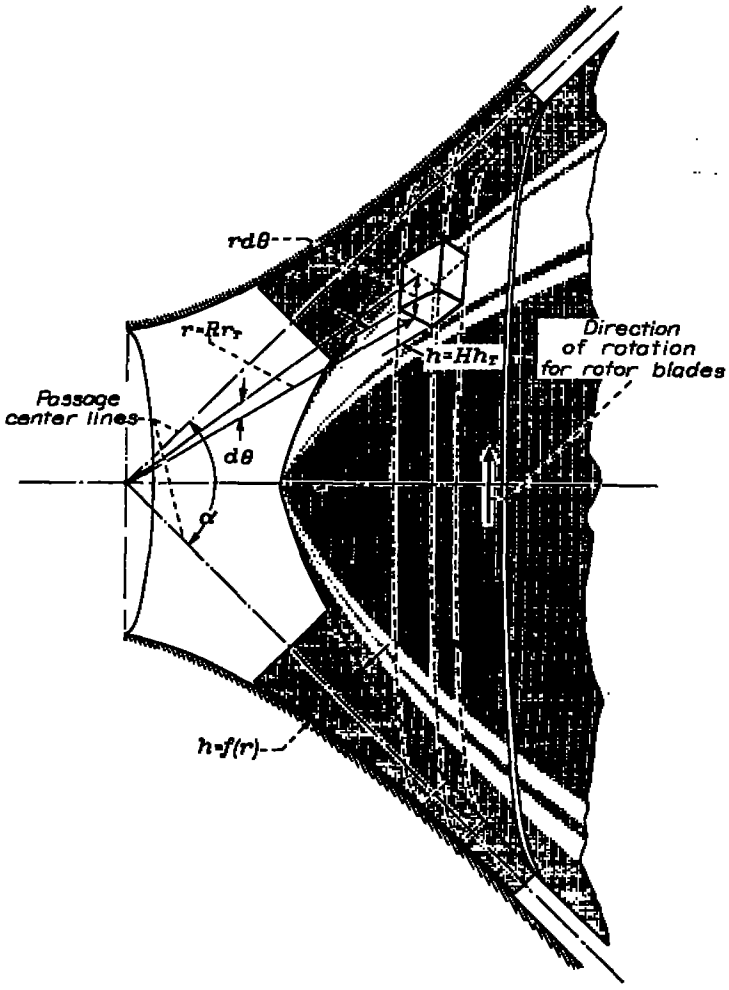

FIGURE 1.—Fluid particle on coordinate system relative to blades. Blades may be stationary (stator blades) or rotating (rotor blades). Center line of flow passage generates surface of right circular cone with cone angle α.

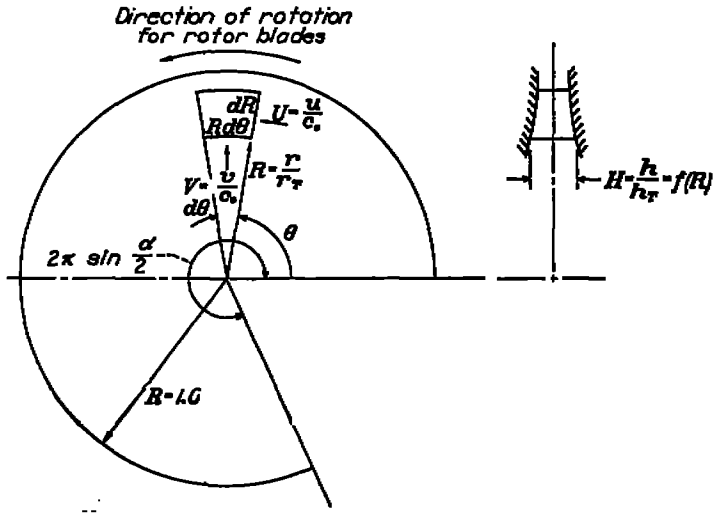

FIGURE 2.—Fluid particle on developed view of conic flow surface. This surface may be stationary (stator blades) or rotating (rotor blades). R and θ, dimensionless coordinates relative to blades; H, passage-height ratio normal to conic flow surface; U and V, tangential and radial components, respectively, of relative velocity ratio Q.

the blades. The blades, and therefore the coordinate system, may be stationary (stator blades) or rotating (rotor blades). The conic-radius ratio R is defined as

$$R=\frac{r}{r_T} \tag{1}$$

where r is the conic radius (distance along conic element from apex of cone) and where the subscript T refers to the blade tip (either the nose or the tail of the blade, whichever has the larger conic radius). The passage-height ratio H (figs. 1 and 2) is normal to the conic flow surface and is a continuous function of the conic-radius ratio R

$$H=\frac{h}{h_T}=f(R) \tag{2}$$

where h is the passage height at any conic-radius ratio R.

Velocity ratios.—A fluid particle on a developed conic flow surface has a relative tangential-velocity ratio U (fig. 2) and a radial-velocity ratio V (fig. 2) that are related to the relative velocity ratio Q by

$$Q=\frac{q}{c_0}=(U^2+V^2)^{1/2} \tag{3a}$$

where

$$U=\frac{u}{c_0} \tag{3b}$$

$$V=\frac{v}{c_0} \tag{3c}$$

where

c local speed of sound
q velocity of fluid relative to blades
u tangential component of q (positive in direction of increasing θ)
v radial (along conic element) component of q (positive in direction of increasing conic-radius ratio)

Subscript:

o absolute stagnation condition in region of uniform flow upstream of blades

The relative velocity ratio Q is defined on a coordinate system that is relative to the blades, therefore the velocity q (and u) is *absolute* for a stationary coordinate system (stator blades) and *relative* for a rotating coordinate system (rotor blades).

Assumptions and limitations.—This analysis assumes that the flow varies only along the conic flow surface, that is, that flow conditions are uniform across the passage normal to the conic flow surface. In order to satisfy this assumption it is necessary that: (1) The gradient of h with respect to r be small; and (2) the cone angle α (fig. 1) be sufficiently large. The allowable variation in α from 180° will depend on the relative magnitudes of h and r and on the desired accuracy. For small values of α the flow must be assumed to exist in concentric annuli, each with negligible passage height. For the hypothetical limiting case in which the ratio h/r approaches zero everywhere along the conic flow surface, the analysis is accurate for all values of α.

The analysis assumes that steady flow exists relative to the blades. The relative motion between stator and rotor blades introduces pulsations that make the flow unsteady. These pulsations rapidly diminish, however, as the stators and the rotors are moved apart so that the relative flow may be treated as steady (between boundaries, which are far enough upstream and downstream of the blades to obtain uniform flow) provided the stators and the rotors are not too close together.

DIFFERENTIAL EQUATIONS FOR FLOW IN $R\theta$-PLANE

The differential equations for steady, two-dimensional, compressible flow are developed from the continuity equation, the equation for absolute irrotational motion, and the general energy equation.

Continuity and stream function.—From steady-flow continuity considerations for the fluid particle in figure 2

$$\left(\frac{\rho}{\rho_o} VHR\right)_R+\left(\frac{\rho}{\rho_o} UH\right)_\theta=0 \tag{4}$$

where ρ is the weight density of the fluid, and where the coordinate subscripts (R and θ, in this case) refer to partial derivatives with respect to the coordinates.

A dimensionless stream function ψ satisfies the continuity equation (4) if defined as

$$\psi_\theta=\frac{\rho}{\rho_o} VHR \tag{4a}$$

and

$$\psi_R=-\frac{\rho}{\rho_o} UH \tag{4b}$$

Absolute irrotational motion.—In the absence of viscosity, shock, nonuniform heat addition, and so forth, the absolute motion of a fluid particle is irrotational. The dimensionless absolute circulation $d\Gamma$ about the particle in figure 2 is therefore zero, and

$$d\Gamma=0=[(RM_T+U)Rd\theta]_R dR-[VdR]_\theta d\theta$$

where the blade-tip Mach number M_T is defined by

$$M_T=\frac{\omega r_T \sin\frac{\alpha}{2}}{c_o} \tag{5}$$

where ω is the angular velocity of the rotor and where (RM_T+U) is the tangential component of the absolute velocity ratio. (For stator blades M_T is zero.) After simplification,

$$-2M_T=\frac{U}{R}+U_R-\frac{V_\theta}{R} \tag{6}$$

Substitution of the stream function ψ as defined by equations (4a) and (4b) gives

$$2M_T H\frac{\rho}{\rho_o}=\psi_{RR}+\frac{\psi_R}{R}+\frac{\psi_{\theta\theta}}{R^2}-\psi_R(\log_e H)_R-\psi_R\left(\log_e\frac{\rho}{\rho_o}\right)_R-\frac{\psi_\theta}{R^2}\left(\log_e\frac{\rho}{\rho_o}\right)_\theta \tag{7}$$

where the double coordinate subscripts (RR and $\theta\theta$, in this case) refer to second partial derivatives with respect to the coordinates.

General energy equation.—The general energy equation is used to determine the density ratio ρ/ρ_o in the differential equation (7). When expressed in terms of the velocity ratios defined by equations (3b) and (3c), the general energy equation becomes

$$Jc_pT+\frac{c_o^2}{2g}[(RM_T+U)^2+V^2]=Jc_pT_o+\frac{M_Tc_o^2}{g}(\lambda-\lambda_U) \tag{8}$$

where

J mechanical equivalent of heat
c_p specific heat at constant pressure
T static (stream) temperature
g gravitational acceleration

Subscript:

U upstream boundary (boundary in region of uniform flow upstream of blades)

and where the "whirl" ratio λ is defined by

$$\lambda=R(RM_T+U) \tag{9}$$

which is the whirl or absolute moment of momentum $\left(\text{radius times absolute tangential velocity}, r\sin\frac{\alpha}{2}\times\left(\omega r\sin\frac{\alpha}{2}+u\right)\right)$ divided by a constant $\left(r_T\sin\frac{\alpha}{2}\times c_o\right)$. The last term in equation (8) is the work done on the fluid and is equal to $\frac{M_Tc_o^2}{g}$ times the change in whirl ratio. The total work done on the fluid is given by the last term in equation (8) with λ equal to λ_D (where subscript D refers to downstream boundary, the boundary in the region of uniform flow downstream of the blades). This total work is positive for compressors and

negative for turbines. The whirl ratios λ_U and λ_D are constant in the uniform flow regions upstream and downstream of the blades (constant absolute moment of momentum).

Rearrangement of equation (8) with

$$c_o^2=(\gamma-1)Jgc_pT_o$$

where γ is the ratio of specific heats, results in

$$\frac{T}{T_o}=1+\frac{\gamma-1}{2}\left[(R\bar{M}_T)^2-Q^2-2\bar{M}_T\lambda_U\right] \tag{10}$$

from which

$$\frac{\rho}{\rho_o}=\left(\frac{T}{T_o}\right)^{\frac{1}{\gamma-1}}=\left\{1+\frac{\gamma-1}{2}\left[(R\bar{M}_T)^2-Q^2-2\bar{M}_T\lambda_U\right]\right\}^{\frac{1}{\gamma-1}} \tag{11}$$

Also, from equations (3a), (4a), and (4b)

$$Q\frac{\rho}{\rho_o}=\left[\left(\frac{\psi_R}{H}\right)^2+\left(\frac{\psi_\theta}{HR}\right)^2\right]^{1/2} \tag{12}$$

Equations (11) and (12) together with the general differential equation (7) provide three equations with three unknowns: ψ, Q, and ρ/ρ_o. The solution of these equations determines the steady, two-dimensional flow of compressible fluid through turbomachines with arbitrary blade shape, with arbitrary variation in the passage-height ratio, and with constant cone angle.

METHOD OF SOLUTION

Equation (7), which is nonlinear, can be solved (together with equations (11) and (12)) by relaxation methods.

Relaxation methods.—Values of ψ are estimated at each point of a grid system placed within the boundaries of the problem, and the residuals R, which result from the estimated values of ψ, are computed for each grid point by expressing the differential equation for ψ in finite-difference form with the sum of all terms equal to R instead of zero. The solution is then obtained by systematically varying (relaxing) the values of ψ at the grid points inside the boundaries until the values of R approach zero.

Transformation of coordinates.—For the numerical solution of this problem by relaxation methods, it is convenient (but not necessary) to select a new set of coordinates (reference 8) so that blades of arbitrary shape in the physical plane (R,θ coordinates) become thin, straight, and parallel in the transformed plane (ξ,η coordinates). Thus a grid of equally spaced points can be placed between the blades. This transformation of coordinates is represented by the general analytic function

$$\xi(R,\theta)+i\eta(R,\theta)=f[R\ exp\ (i\theta)] \tag{13}$$

where the Cartesian coordinates ξ and η in the $\xi\eta$-plane correspond to velocity potential lines (ξ=constant) and stream lines (η=constant) in the $R\theta$-plane for incompressible flow past the blades, which, for purposes of the transformation, are considered to be stationary ($\omega=0$) and to have a constant height ($H=1$). Equation (13), in specific form for a given blade shape, determines ξ and η as functions of R and θ

$$\left.\begin{aligned}\xi&=\xi(R,\theta)\\ \eta&=\eta(R,\theta)\end{aligned}\right\} \tag{13a}$$

Equation (7), in terms of the transformed coordinates ξ and η given by equation (13a), becomes (appendix B)

$$\frac{2\bar{M}_TH}{q_i^2}\frac{\rho}{\rho_o}=\psi_{\xi\xi}+\psi_{\eta\eta}-\psi_\xi\left(\log_e\frac{\rho}{\rho_o}\right)_\xi-\psi_\eta\left(\log_e\frac{\rho}{\rho_o}\right)_\eta-\frac{(\psi_\xi v_i-\psi_\eta u_i)}{q_i^2}\left[(\log_e H)_\xi v_i-(\log_e H)_\eta u_i\right] \tag{14}$$

and equation (12) becomes

$$Q\frac{\rho}{\rho_o}=\frac{q_i}{H}(\psi_\xi^2+\psi_\eta^2)^{1/2} \tag{15}$$

where H is now a function of ξ and η (given by equations (2) and (13a)) and where the coefficients u_i, v_i, and q_i are derivatives of equation (13a) defined by

$$u_i=-\eta_R=\frac{\xi_\theta}{R} \tag{16a}$$

$$v_i=\frac{\eta_\theta}{R}=\xi_R \tag{16b}$$

$$q_i=(u_i^2+v_i^2)^{1/2} \tag{16c}$$

where the subscript i indicates that the coefficients correspond to incompressible velocities in the $R\theta$-plane.

For certain simple blade shapes, equation (13) is a simple analytic expression that determines $\xi(R,\theta)$ and $\eta(R,\theta)$ (equations (13a)) directly. For arbitrary blade shapes, however, a specific expression for equation (13) is not readily available and it is easier to obtain $\xi(R,\theta)$ and $\eta(R,\theta)$ by relaxation solutions of the Laplace equations for ξ and η in the $R\theta$-plane (appendix C).

Finite-difference equations.—In order to solve the system of equations (equations (11), (14), and (15)) by relaxation methods, equations (14) and (15) must first be changed to finite-difference form. This change is accomplished with the aid of the following equations (reference 7, p. 19), which are based on first-order differences: (Note that higher-order differences could be used, which would result in more complex finite-difference equations but which would enable larger grid spacing, and therefore fewer grid points, for the same degree of approximation.)

$$\left.\begin{aligned}F_\xi&\approx\frac{1}{2b}(F_1-F_3)\\ F_\eta&\approx\frac{1}{2b}(F_2-F_4)\\ F_{\xi\xi}&\approx\frac{1}{b^2}(F_1+F_3-2F)\\ F_{\eta\eta}&\approx\frac{1}{b^2}(F_2+F_4-2F)\end{aligned}\right\} \tag{17}$$

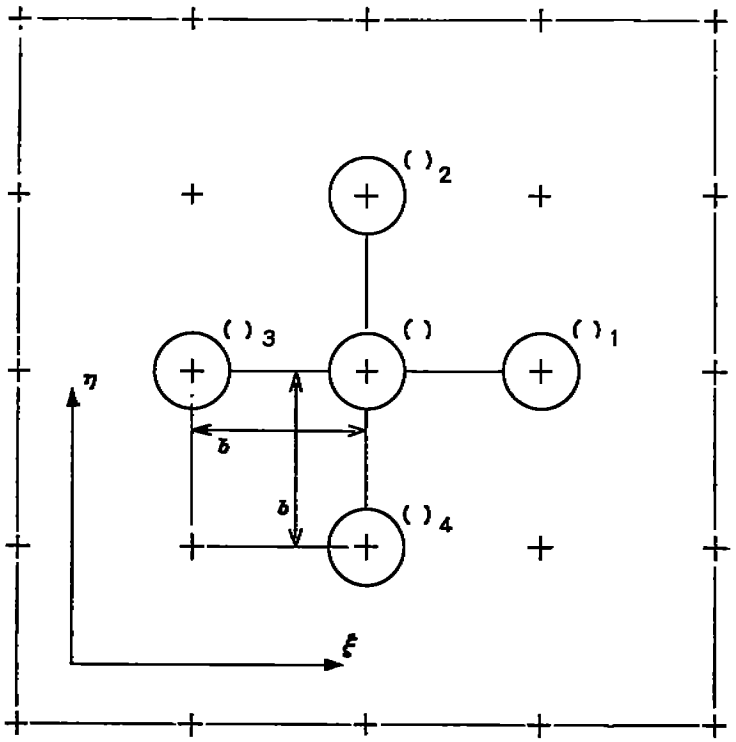

FIGURE 3.—Sample grid showing grid spacing b and numerical subscript convention for adjacent grid points.

where

F any twice-differentiable function of two variables (ξ and η, in this case)

b grid spacing

Subscripts:

1, 2, 3, 4 grid points adjacent to point being considered (F with no subscript)

A sample grid is shown in figure 3. The grid spacing b is arbitrary. However, the smaller the value of b, that is, the larger the number of grid points, the greater is the accuracy of the approximate, finite-difference equations (17).

With the aid of equations (17), equation (14) becomes

$$\psi_1+\psi_2+\psi_3+\psi_4-4\psi-\frac{(\psi_1-\psi_3)}{4}\left(\log_e\frac{\rho_1}{\rho_e}-\log_e\frac{\rho_3}{\rho_e}\right)-$$

$$\frac{(\psi_2-\psi_4)}{4}\left(\log_e\frac{\rho_2}{\rho_e}-\log_e\frac{\rho_4}{\rho_e}\right)-$$

$$\frac{1}{4q_i^2}\left[(\psi_1-\psi_3)v_i-(\psi_2-\psi_4)u_i\right]\times$$

$$\left[(\log_e H_1-\log_e H_3)v_i-(\log_e H_2-\log_e H_4)u_i\right]-$$

$$\frac{2M_THb^2}{q_i^2}\frac{\rho}{\rho_e}=\mathrm{R} \tag{18}$$

where the residual R has a nonzero value when the values of ψ do not satisfy the differential equation (14) from which equation (18) was obtained.

Equation (15) in finite-difference form becomes

$$Q\frac{\rho}{\rho_e}=\frac{q_i}{2bH}\left[(\psi_1-\psi_3)^2+(\psi_2-\psi_4)^2\right]^{1/2} \tag{19}$$

After the values of ψ have been estimated at the grid points inside the boundaries, the system of equations (11), (18), and (19) provides three equations with three unknowns $\frac{\rho}{\rho_e}$, Q, and R at each grid point. Equations (11) and (19) determine the values of the density ratios in equation (18), which is then solved for the residual R.

BOUNDARY CONSIDERATIONS

The values of ψ at the grid points inside the boundaries depend upon the values of ψ at the grid points along the boundaries. These boundary values of ψ are determined by the design characteristics and the operating conditions of the turbomachine.

Location of boundaries.—The boundaries of the flow field in the $R\theta$-plane (fig. 4(a)) are the blade surfaces and the upstream and downstream boundaries at constant values of R, which are any distance far enough from the blades to insure uniform flow conditions at these boundaries. The upstream and downstream boundaries enclose all the blades;

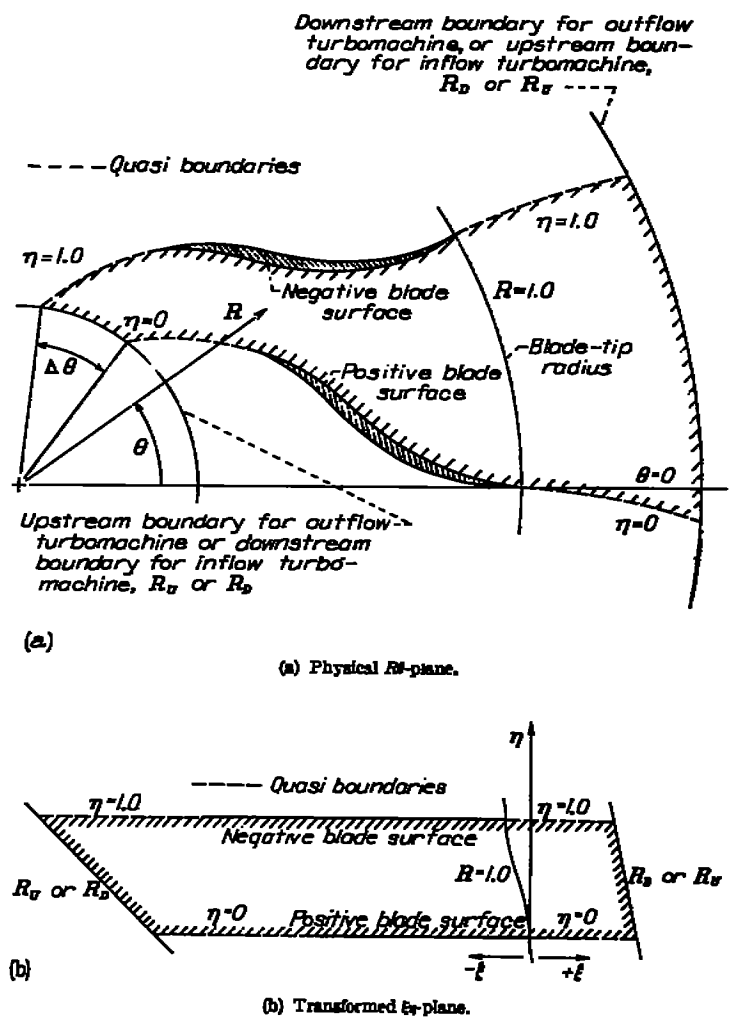

(a) Physical $R\theta$-plane.

(b) Transformed $\xi\eta$-plane.

FIGURE 4.—Boundaries of typical two-dimensional flow field for arbitrary blade shape.

however, from symmetry considerations, the flow conditions along lines of constant R are cyclic with a period equal to the blade spacing so that the solution need be obtained only in a region that encloses the equivalent flow between two blades. This region is bounded by any two blades, the upstream and downstream boundaries, and by quasi boundaries between the two blades and the upstream and downstream boundaries (fig. 4(a)). These quasi boundaries may have any reasonable, continuous shape but must have the same angular spacing $\Delta\theta$ (fig. 4(a)) as the blades, where

$$\Delta\theta=\frac{2\pi}{B}\sin\frac{\alpha}{2} \tag{20}$$

where B is the number of blades (or passages). It is convenient to select as the shape of these quasi boundaries the incompressible, stagnation streamlines (constant η) that are determined in appendix C with stagnation points at the nose and the tail of the blade.

In the $\xi\eta$-plane (fig. 4(b)), the blade surfaces become lines of constant η and the quasi boundaries become extensions of these same lines. The upstream and downstream boundaries in the $\xi\eta$-plane are straight (appendix C) but, in general, are not at right angles to the lines of constant η. The two blade surfaces are generally different lengths in this plane (fig. 4(b)).

ψ along blade boundaries.—The boundary values of ψ along the blade surfaces are constant and can be determined from the following considerations:

The differential flow rate between adjacent streamlines is shown in figure 5 and is given by

$$dw=\rho v h_T r_T HRd\theta-\rho u h_T r_T HdR$$

where w is the flow rate between streamlines. From equations (3b), (3c), (4a), and (4b),

$$dw=\rho_e c_e h_T r_T(\psi_\theta d\theta+\psi_R dR)$$

or

$$dw=\rho_e c_e h_T r_T d\psi \tag{21}$$

If w and ψ are assigned values of zero along the positive blade surface (the blade surface in the direction of increasing θ), equation (21) can be integrated across the passage to the negative blade surface (the blade surface in the direction of decreasing θ) to give

$$\frac{W}{B}=\rho_e c_e h_T r_T \psi_n \tag{22}$$

where W is the total flow rate through the turbomachine and the subscript n refers to the negative blade surface. Equation (22) can be simplified by the following considerations:

The flow area a_T of the annulus at the tip of the blades is given by

$$a_T=2\pi\sin\frac{\alpha}{2}r_T h_T$$

from which equation (22) combined with equation (20) becomes

$$\psi_n=\phi\Delta\theta \tag{23}$$

where the flow coefficient ϕ is defined by

$$\phi=\frac{W}{\rho_e a_T c_e} \tag{24}$$

Equation (23) determines the boundary value of ψ on the negative blade surface as a function of the operating parameter ϕ and the design parameter $\Delta\theta$.

Equation (23) was developed for through flow in the direction of increasing radius ratio (outflow turbomachines), that is, for positive values of the radial-velocity ratio V. For through flow in the direction of decreasing radius ratio (inflow turbomachines), that is, negative values of V, the magnitude of ψ_n is given by equation (23) but the sign is changed from positive to negative.

ψ along quasi boundaries extending from positive blade surface.—Because the quasi boundaries in the $\xi\eta$-plane enclose the equivalent flow between two blades (see section **Location of boundaries**), the values of ψ at points along the quasi boundaries extending from the negative blade surface (fig. 4(b)) are ψ_n greater (outflow machine), or ψ_n less (inflow machine) than the values of ψ at corresponding grid points (corresponding to the same value of R) along the quasi boundaries extending from the positive blade surface. Therefore, the values of ψ along the quasi boundaries extending from the negative blade surface are not recorded or relaxed.

Estimated values of the stream function ψ along the quasi boundaries extending from the positive blade surface in the $\xi\eta$-plane (fig. 4(b)) can be obtained by assuming, as a first

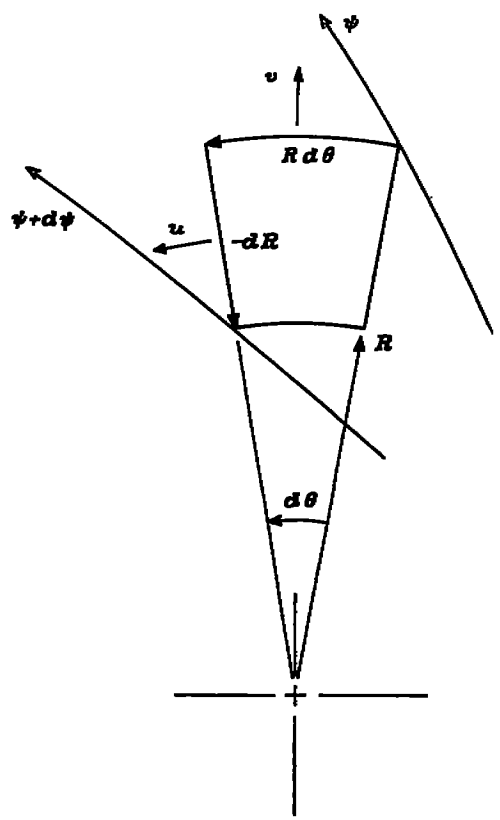

FIGURE 5.—Fluid particle between adjacent streamlines. Radial component of flow rate, $\rho v h_T r_T HRd\theta$; tangential component of flow rate, $-\rho u h_T r_T HdR$.

approximation, that the flow conditions upstream and downstream of the blades in the $R\theta$-plane (fig. 4(a)) are uniform, that is, the flow conditions are a function of only R. The variation in ψ with ξ along the quasi boundaries extending from the positive blade surface can then be determined (appendix D) from continuity and from the whirl ratios λ_U and λ_D, which for uniform flow remain constant upstream and downstream of the blades (conservation of moment of momentum). The whirl ratio λ_U is specified and the whirl ratio λ_D is determined, for a given blade shape and operating condition, by the Joukowski condition, which requires that the rear stagnation point occur at the blade tail (or, in the case of infinitely thin blades or blades with cusped tails, the flow must be tangent to the blade surfaces at the tail). The value of λ_D can be estimated from considerations given in appendix D.

The values of ψ along the quasi boundaries extending from the positive blade surface (which values are obtained from the preceding variation in ψ with ξ) are estimated values and must therefore be relaxed.

ψ along upstream and downstream boundaries.—The value of ψ at any point along the upstream or downstream boundary (fig. 4(b)) is determined by the integrated variation in ψ along the quasi boundary from the fixed (zero) value of ψ on the positive blade surface and by the integrated variation in ψ along the upstream or downstream boundary to the point in question. The variation in ψ along the quasi boundaries was estimated in the previous section, and the variation in ψ along the upstream and downstream boundaries is constant (uniform flow conditions assumed at these boundaries) and is of such magnitude that the change in ψ from one quasi boundary to the next is equal to ψ_s.

The values of ψ along the upstream and downstream boundaries (ψ_U and ψ_D, respectively) are considered fixed during a relaxation solution. But these values of ψ, for the initial relaxation solution, are dependent upon the estimated variation in ψ along the quasi boundaries extending from the positive blade surface. In general, therefore, these values of ψ_U and ψ_D do not result in a solution that exactly satisfies the prescribed whirl ratio λ_U upstream of the blades and the Joukowski condition (which, together with the blade shape and the operating conditions, determines λ_D) downstream of the blades. It is therefore usually necessary, after the initial relaxation solution, to adjust (by methods developed in appendixes E and F) the values of ψ_U and ψ_D (keeping, however, the same uniform variation in ψ along these boundaries). The relaxation solution is then repeated using these new values of ψ_U and ψ_D that satisfy λ_U and the Joukowski condition.

ADDITIONAL CONSIDERATIONS

Equivalent turbomachines with different cone angles.—The flow field for the flow that passes between any two blades is the same for all blade passages in a given turbomachine. Therefore, the solution obtained for the flow field in a given turbomachine also applies to certain other (equivalent) turbomachines with a larger or smaller number of like passages having the same angular spacing of the blades $\Delta\theta$, blade-thickness distribution, and so forth, but with different cone angles α. The cone angles for the equivalent turbomachines are determined by the number of passages B in the machine and are given by equation (20) as

$$\alpha=2\sin^{-1}\frac{B\Delta\theta}{2\pi}$$

Also, from equation (20),

$$B=\frac{2\pi}{\Delta\theta}\sin\frac{\alpha}{2}$$

so that a radial-flow turbomachine ($\alpha=180°$) has more blades than an equivalent mixed-flow turbomachine ($\alpha<180°$), which has the same blade loading, and so forth. Furthermore, if the number of blades in the equivalent mixed-flow turbomachine is increased to equal the number of blades in the radial-flow turbomachine, the blade loading in the mixed-flow machine is decreased, so that, in general, for the same number of similar blades, the blade loading is less for mixed-flow than for radial-flow turbomachines.

Equivalent outflow and inflow turbomachines.—Any solution obtained for an outflow turbomachine with shockless (smooth) entry is also a solution for an inflow turbomachine with shockless entry and with the flow direction and blade rotation (if any) reversed. The shockless entry for the outflow machine corresponds to the Joukowski condition for the inflow machine and, vice versa.

Axial-flow turbomachines.—For axial-flow turbomachines, the cone angle α becomes zero and the flow field is assumed to lie on a cylindrical surface about the axis of the machine. For a cylindrical surface, the conic radius r is infinite and therefore the angle θ is zero. As a result, the cylindrical flow surface degenerates into a single point (1,0) on the developed conic flow surface (R,θ) in figure 2, so that no solution can be obtained for axial-flow turbomachines on the developed conic flow surface for which this analysis was developed.

NUMERICAL PROCEDURE

A detailed outline of the numerical procedures for the relaxation solution of compressible-flow problems is given in reference 8. The emphasis is placed herein on those features of the solution that are peculiar to the flow in turbomachines with conic flow surfaces.

The complete relaxation solution is conveniently divided into two sections. In the first section, the initial relaxation solution is obtained using approximate values of ψ_D and ψ_U that are estimated to satisfy the Joukowski condition and the prescribed whirl ratio λ_U. In the second section, the approximate values of ψ_D and ψ_U are adjusted to satisfy the Joukowski condition and the prescribed λ_U, and the final relaxation solution is obtained. A brief outline of the numerical procedure for the initial relaxation solution follows.

I—INITIAL RELAXATION SOLUTION

Design characteristics and operating conditions.—In order to solve the system of equations (11), (14), and (15) for the stream function ψ, it is necessary that the following design characteristics and operating conditions be specified:

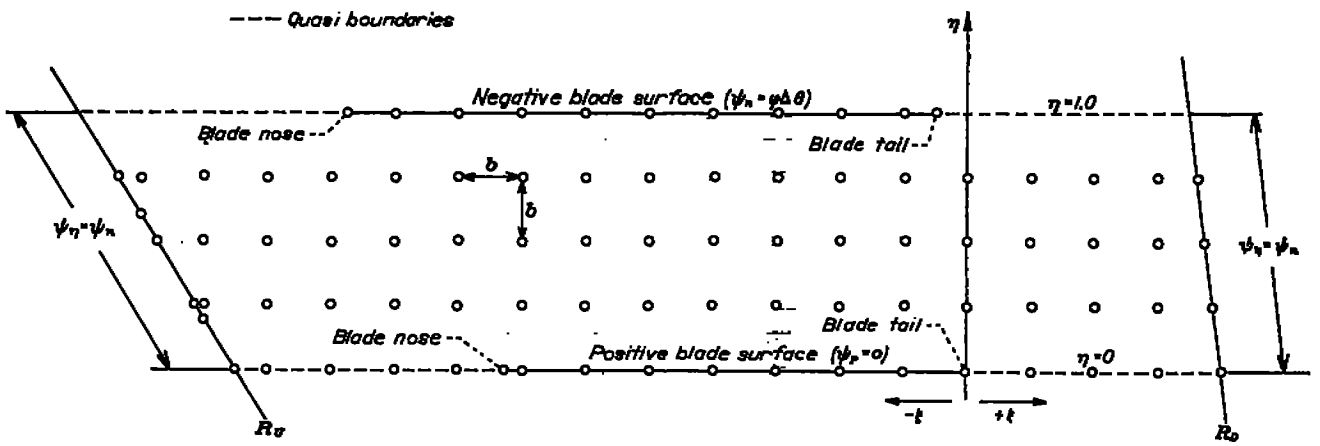

FIGURE 6.—Grid layout for outflow turbomachine on transformed $\xi\eta$-plane

Design characteristics:

(1) Passage-height ratio H, which is a function of the conic-radius ratio R

$$H=f(R) \tag{2}$$

(2) Cone angle α, which is constant (fig. 1)

(3) Arbitrary blade shape, which determines (appendix C)

$$\left.\begin{aligned}\xi&=\xi(R,\theta)\\ \eta&=\eta(R,\theta)\end{aligned}\right\} \tag{13a}$$

from which the coefficients u_i, v_i, and q_i in equations (14) and (15) are obtained by equations (16a), (16b), and (16c), respectively.

(4) Number of blades B, which together with the cone angle α, determines the angular blade spacing $\Delta\theta$

$$\Delta\theta=\frac{2\pi}{B}\sin\frac{\alpha}{2} \tag{20}$$

Operating conditions:

(5) Whirl ratio upstream of blades λ_U, where λ is defined by

$$\lambda=R(RM_T+U) \tag{9}$$

The value of λ_U results from the configuration of the turbomachine ahead of the blades (design characteristic) and from the flow rate through the machine (operating condition).

(6) Tip Mach number M_T, which is defined as

$$M_T=\frac{\omega r_T\sin\frac{\alpha}{2}}{c_0} \tag{5}$$

For stator blades M_T is zero.

(7) Flow coefficient ϕ, which is defined as

$$\phi=\frac{W}{\rho_0 a_T c_0} \tag{24}$$

This coefficient is proportional to the standard equivalent flow-rate parameter $W\sqrt{\theta}/\delta$ (reference 9) where

θ ratio of upstream absolute stagnation temperature to standard sea-level temperature

δ ratio of upstream absolute stagnation pressure to standard sea-level pressure

(8) Ratio of specific heats γ, which for a given problem is considered constant

Boundary values of ψ.—The locations of the boundaries in the $\xi\eta$-plane are discussed under **Location of boundaries** in the section **ANALYSIS**. The boundary values of ψ are determined by the design characteristics and operating conditions outlined in the previous section and by the Joukowski condition. The various boundary values of ψ are shown on the relaxation grid for an outflow turbomachine in the $\xi\eta$-plane in figure 6. The manner in which these boundary values are obtained is summarized as follows:

(1) The value of the stream function along the positive blade surface in figure 6 is arbitrarily set equal to zero. (See section **ψ along blade boundaries.**)

(2) The value of the stream function along the negative blade surface in figure 6 is given by

$$\psi_n=\phi\Delta\theta \tag{23}$$

The stream function ψ_n is positive for outflow turbomachines and negative for inflow machines. (See section **ψ along blade boundaries.**)

(3) The values of the stream function along the quasi boundaries extending upstream and downstream of the positive blade surface depend on the specified whirl ratio λ_U upstream of the blades and, for a given blade shape and operating conditions, on the Joukowski condition downstream of the blades. The method for estimating ψ along these quasi boundaries is given in appendix D. Values of ψ are not recorded or relaxed along the quasi boundaries extending from the negative blade surface for reasons given in the section **ψ along quasi boundaries extending from positive blade surface.**

(4) The values of the stream function along the upstream and downstream boundaries vary uniformly (steady-flow condition) in the direction of increasing η at the rate of ψ_n per unit of η. (This rate is positive for outflow turbomachines and negative for inflow machines.) The magnitude of ψ is fixed at the intersection of the quasi boundaries

(extending from the positive blade surface) with the upstream or downstream boundary by the variation in ψ along these quasi boundaries.

Grid layout.—A system of equally spaced grid points placed on the flow field in the $\xi\eta$-plane is shown in figure 6. The grid spacing b is selected so that an integral number of spacings occur between the blades. The smaller the grid spacing, the greater is the accuracy of the finite-difference equations (18) and (19), but also, the greater is the number of grid points and therefore the labor involved in obtaining the solution.

For reasons given in the section **ψ along quasi boundaries extending from positive blade surface**, grid points are not located on the quasi boundaries extending from the negative blade surface.

It is convenient (appendix E) to locate the grid system so that a grid point lies at the blade tail on the positive blade surface. In this case, the grid point on the blade nose of the positive blade surface is generally not equally spaced from the interior grid points. Also, because the upstream and downstream boundaries are not normal, in general, to the ξ-axis (fig. 6), the grid points on these boundaries are usually not equally spaced from the interior grid points. In order to account for these unequal spacings of the boundary grid points, the finite-difference equations (18) and (19) must be modified at the adjacent interior grid points (to be subsequently discussed).

After estimating (or assuming) the values of ψ at the interior grid points, the problem resolves itself into two parts: (1) calculation of the residuals R at the interior grid points and along the quasi boundaries extending from the positive blade surface (which residuals result from the estimated values of ψ at these points); and (2) relaxation (elimination) of these residuals by suitable adjustments in the values of ψ at these grid points.

Residuals.—The residuals at equally spaced interior points of the grid system are computed from equation (18). The density ratios in equation (18) are determined by equation (11) with the aid of equation (19). At the interior grid points adjacent to the blade surfaces, the solution of equation (18) requires the density ratios at the grid points on the blade surfaces; these ratios can be determined by extrapolating the values of ρ/ρ_0 obtained at interior grid points or by equations (11) and (19) at the boundary grid points using extrapolated values of ψ beyond the boundaries.

In general, the grid points along the upstream and downstream boundaries are unequally spaced from the adjacent interior grid points (fig. 6) so that at these interior grid points the finite-difference equations (18) and (19) must be modified to account for the unequal grid spacing (reference 7, pp. 73–74). This unequal grid spacing also exists, in general, between the nose of the positive blade surface and the adjacent grid point on the quasi boundary (fig. 6).

In order to compute the residuals at grid points along the quasi boundaries extending from the positive blade surface (fig. 6), equations (18) and (19) require values of ψ_4 that lie outside the flow field enclosed by the quasi boundaries (fig. 7). From symmetry considerations and because the quasi boundaries enclose the equivalent flow between two blades (see section **Location of boundaries**), the values of ψ_4 equal ψ_R less (or greater, for inflow turbomachines) than the values of ψ at corresponding positions (same value of R, that is, same increment of ξ from the tail, or nose, of the blades) along the row of interior grid points adjacent to the quasi boundary extending from the negative blade surface. That is,

$$\psi_4=\psi_A-\psi_R \tag{25}$$

where ψ_A, corresponding to ψ_4 for a given grid point along the quasi boundary extending from the positive blade surface, is shown in figure 7. In general, ψ_A does not lie on a grid point and the value of ψ_A is therefore obtained by linear interpolation between the adjacent grid points ψ_B and ψ_C (fig. 7). Therefore,

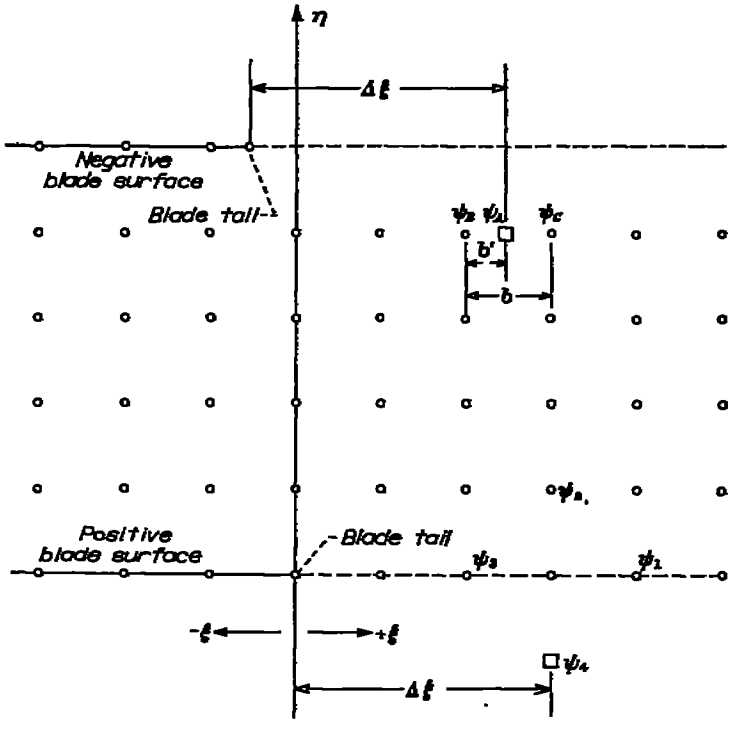

FIGURE 7.—Relaxation grid in $\xi\eta$-plane showing values of ψ used in equation (27).

$$\psi_A=\psi_B+(\psi_C-\psi_B)\frac{b'}{b} \tag{26}$$

where b' is defined in figure 7. From equations (25) and (26),

$$\psi_4=\psi_B-\psi_R+\frac{b'}{b}(\psi_C-\psi_B) \tag{27}$$

Equation (27) determines the value of ψ_4 required by equations (18) and (19) in order to compute the residuals along the quasi boundaries extending from the positive blade surface.

If all the estimated values of ψ are correct, the value of R is zero at all grid points. If, however, the estimated values of ψ are incorrect, the values of R are finite and may be positive or negative.

Relaxation.—After the residuals are computed, it remains to relax (that is, reduce) these residuals by suitable changes in the values of ψ. In order to determine the magnitude

of the required changes in ψ at the equally spaced interior grid points, all terms of the finite-difference equation (18) are assumed to remain constant except the terms $\psi_1+\psi_2+\psi_3+\psi_4-4\psi$. A change in the value of ψ therefore causes a four-fold change of opposite sign in the value of R, and this change in ψ also causes an equal change in the values of R at each of the adjacent grid points (because relative to these points the change in ψ amounts to a change in ψ_1, ψ_2, ψ_3, or ψ_4). At grid points that are unequally spaced from adjacent points (for example, at the grid points adjacent to the upstream and downstream boundaries, fig. 6) a change in ψ changes R an amount that depends on the coefficient of ψ in the finite-difference form of equation (14) developed for unequal spacing. (See previous section.) Also, the resulting change in R at adjacent grid points depends on the coefficients for the terms ψ_1, ψ_2, ψ_3, and ψ_4 in this finite-difference equation. In particular, it should be noted from equation (27) that changes in ψ_B and ψ_C have a weighted effect upon the residuals at the corresponding adjacent grid points along the quasi boundaries extending from the positive blade surface, and vice versa.

These changes in ψ and R are recorded on the grid sheet as the work progresses. By continually reducing (relaxing) the larger residuals (any desired amount), the values of all residuals gradually approach zero. When this condition is reached, the residuals are recomputed using the complete finite-difference equation and taking into account the new values of the density ratio. After the new values of R have been computed, the relaxation procedure is repeated and this cycle is continued as often as necessary to achieve the desired accuracy.

II—FINAL SOLUTION

The whirl ratio λ_U upstream of the blades and the Joukowski condition downstream of the blades are governed by the values of the stream function specified along the upstream and downstream boundaries (ψ_U and ψ_D). In section I, these values of ψ_U and ψ_D were determined from the estimated variation in ψ along the quasi boundaries extending from the positive blade surface (see section **Boundary values of ψ**) and, in general, do not result in a solution that exactly satisfies the prescribed value of λ_U and the Joukowski condition. In section II, ψ_U and ψ_D are therefore adjusted to satisfy these conditions and the relaxation solution is repeated to obtain the final distribution of ψ in the flow field.

Joukowski condition.—If the Joukowski condition is satisfied, the rear stagnation point occurs at the tail of the blade, or, in case of infinitely thin blades or blades with cusped tails, the flow is tangent to the blade surfaces at the tail. In either case, from appendix E,

$$0=4\psi_a^t-6\psi_b^t+4\psi_c^t-\psi_d^t \qquad \text{(E2)}$$

where ψ^t is the value of ψ after the Joukowski condition is satisfied and where the subscripts a, b, c, and d refer to the

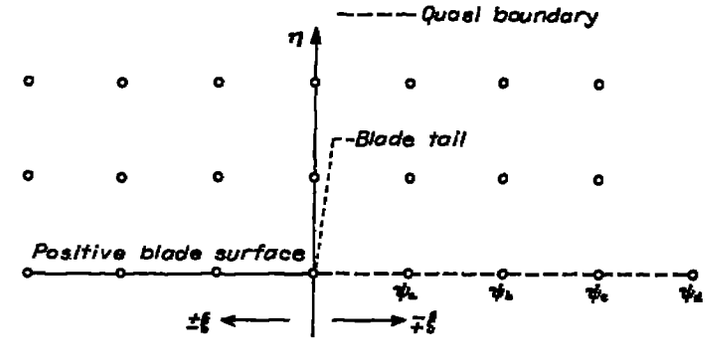

FIGURE 8.—Relaxation grid in $\xi\eta$-plane showing values of ψ used in equation (E2) to check Joukowski condition.

grid points along the quasi boundary extending from the positive blade surface on the $\xi\eta$-plane (shown in fig. 8). If equation (E2) is not satisfied by the values of ψ_a, ψ_b, ψ_c, and ψ_d resulting from the initial relaxation solution (section I), the values of ψ_D along the downstream boundary are adjusted by methods given in appendix E. As a result of adjusting ψ_D, the values of ψ at all other grid points in the flow field are changed by amounts that are estimated by methods developed in appendix E.

Upstream whirl ratio λ_U.—If the upstream whirl ratio is satisfied, the whirl ratio at any point in the region of uniform flow upstream of the blades is equal to the prescribed value λ_U, and ψ_ξ at that point is given by equation (F2) developed in appendix F

$$\psi_\xi^*=\frac{1}{v_i}\left[u_i\psi_\eta-\frac{\rho}{\rho_e}H\left(\frac{\lambda_U}{R}-RM_T\right)\right] \qquad \text{(F2)}$$

where ψ_ξ^* is the value of ψ_ξ if the specified value of λ_U is obtained. In general, equation (F2) is evaluated at the upstream boundary where, because conditions are uniform, ψ_ξ is constant. If ψ_ξ obtained from the initial relaxation solution (section I) is not equal to the value ψ_ξ^* given by equation (F2), the values of ψ_U along the upstream boundary are adjusted by methods given in appendix F. As a result of adjusting ψ_U, the values of ψ at all other grid points in the flow field are changed by amounts that are estimated by methods developed in appendix F.

It should be noted that the corrections for λ_U affect the Joukowski condition, and vice versa. For low-solidity blades these interrelations should be considered, but for high-solidity blades the effect of changes in ψ_D on λ_U and the effect of changes in ψ_U on the Joukowski condition are generally small and can be neglected.

After the values of ψ_D and ψ_U have been adjusted and the resulting changes in ψ at the grid points in the flow field have been estimated, the relaxation methods are repeated to eliminate the small residuals that result from the new values of ψ at the grid points in the flow field. After the correct distribution of ψ has been determined, the pressure and velocity-ratio distributions can be obtained from the density ratio and equations (4a) and (4b). If more detailed infor-

mation of flow conditions in certain regions of the flow field is desired, the grid spacing b can be reduced and the relaxation methods repeated in these regions.

Accuracy.—No quantitative evaluation of the accuracy of relaxation solutions is available (reference 10, p. 176). Because the computed velocities depend on differences in the values of ψ at adjacent grid points, that is, the small difference of large numbers, however, it is important to know the values of ψ with sufficient accuracy to assure the desired accuracy for the velocity calculations. In the numerical examples of the present report, the values of ψ were computed to the nearest 0.00001 compared with the maximum value of ψ, at the negative blade surface, of 0.15700.

NUMERICAL EXAMPLES

Two numerical examples are presented; one for compressible and the other for incompressible flow through the impeller of a centrifugal compressor. Both examples are for the same impeller geometry with the same tip speed and weight flow.

Flow field.—A diagram of the impeller and vaneless portion of the diffuser is shown in figure 9. The cone angle α, shown in figure 9, is 180° (radial-flow compressor), but the solution applies to certain other cone angles less than 180° (mixed-flow compressors) given by equation (20) for an integral number of similar passages B with the same included angle $\Delta\theta$ between blades on the conic flow surface. (See section **Equivalent turbomachines with different cone angles.**) The solutions are obtained in a flow field (fig. 9) that is considered to be unaffected by the inlet configuration of the impeller and by the diffuser vanes (if any); that is, the impeller inlet and the diffuser vanes must be far enough removed not to affect the flow appreciably in the flow field investigated. In this flow field, the impeller blades are thin and straight and the passage-height ratio H varies in such a manner that the flow area normal to the conic flow surface remains constant.

The values of the stream function along the boundary between blades (R=0.6752 in fig. 9) are determined from a simplified analysis (appendix G), which assumes that for straight thin blades the component of the relative flow normal to the blades is zero. This assumption is satisfactory (appendix G) at radius ratios within the impeller sufficiently far from the tip (at radius ratios less than 0.80 for the numerical examples of this report).

Transformation of coordinates.—For thin, straight blades lying on conic radii (elements), the transformation of coordinates is given directly by the analytic function

$$\xi+i\eta=\frac{1}{\Delta\theta}\log_e\left[R\ exp\ (i\theta)\right]$$

from which

$$\xi=\frac{\log_e R}{\Delta\theta}$$

and

$$\eta=\frac{\theta}{\Delta\theta}$$

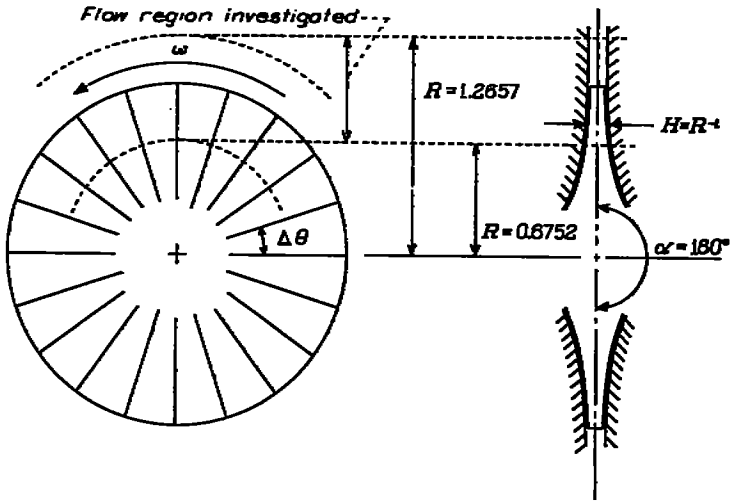

FIGURE 9.—Compressor-design characteristics for numerical examples.

so that, from equations (16a), (16b), and (16c) the coefficients in equations (18) and (19) become

$$u_t=0$$

and

$$v_t=q_t=\frac{1}{R\Delta\theta}$$

Incompressible solution.—The incompressible solution was obtained from equation (18) for the same impeller-tip Mach number M_T and for the same flow coefficient ϕ used in the compressible solution but with the density ratio ρ/ρ_e consant and equal to 1.0. Because for incompressible fluids the speed of sound is infinite, M_T, ϕ, and the velocity ratios for the incompressible solution are fictitious quantities, the definitions of which contain a constant, finite speed of sound that is equal to c_e for the compressible solution. The same value of the impeller-tip speed (and of the compressor flow rate) therefore results from the same value of M_T (and of ϕ) for the compressible and incompressible solutions.

Design characteristics and operating conditions.—The numerical examples have been computed for the following design characteristics and operating conditions:

Design characteristics:

(1) Constant flow area normal to conic flow surface, $H=R^{-1}$
(2) Cone angle α, 180° (or certain other values of α less than 180° given by equation (20) for the same value of $\Delta\theta$ but for different integral values of B)
(3) Straight thin blades along radii
(4) Number of blades B, 20 (or other integral values of B less than 20 for the same value of $\Delta\theta$ but for certain different values of α less than 180° given by equation (20))
(5) Whirl ratio upstream of blades λ_U, 0
(6) Tip Mach number M_T, 1.5
(7) Flow coefficient ϕ, 0.5
(8) Ratio of specific heats γ, 1.4 (for compressible solution only)

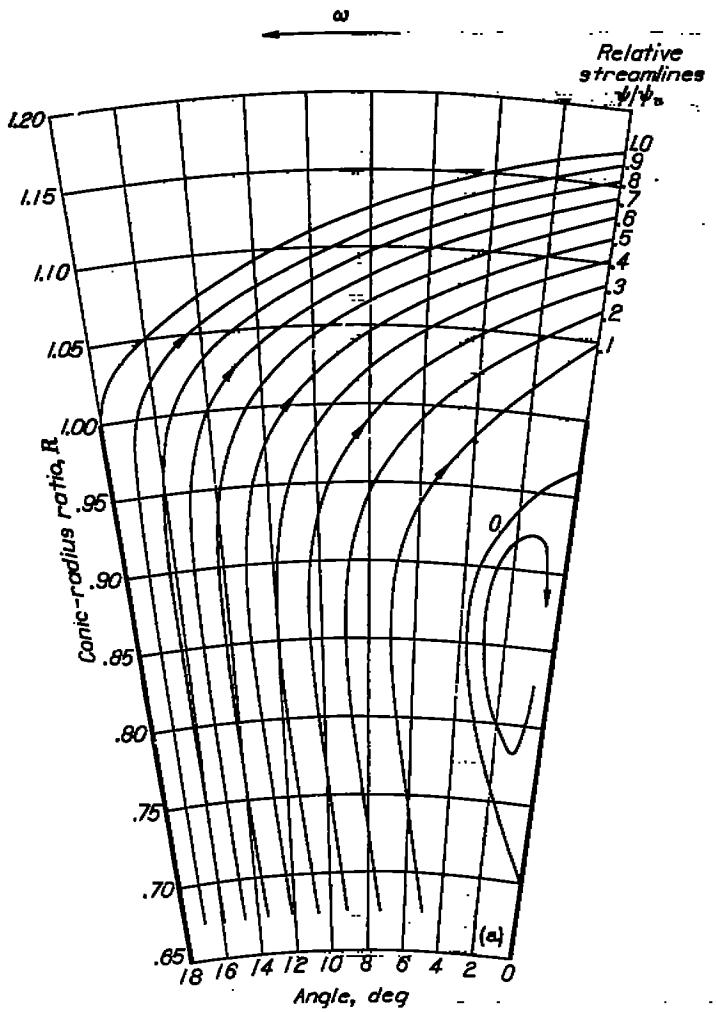

(a) Compressible-flow example.

FIGURE 10.—Relative streamlines for flow through centrifugal compressor with straight blades. Streamline designation indicates ratio of flow between streamline and positive blade surface (right side of passage) to total flow through passage. Angular blade spacing, 18°; impeller-tip Mach number, 1.5; flow coefficient, 0.5; constant flow area.

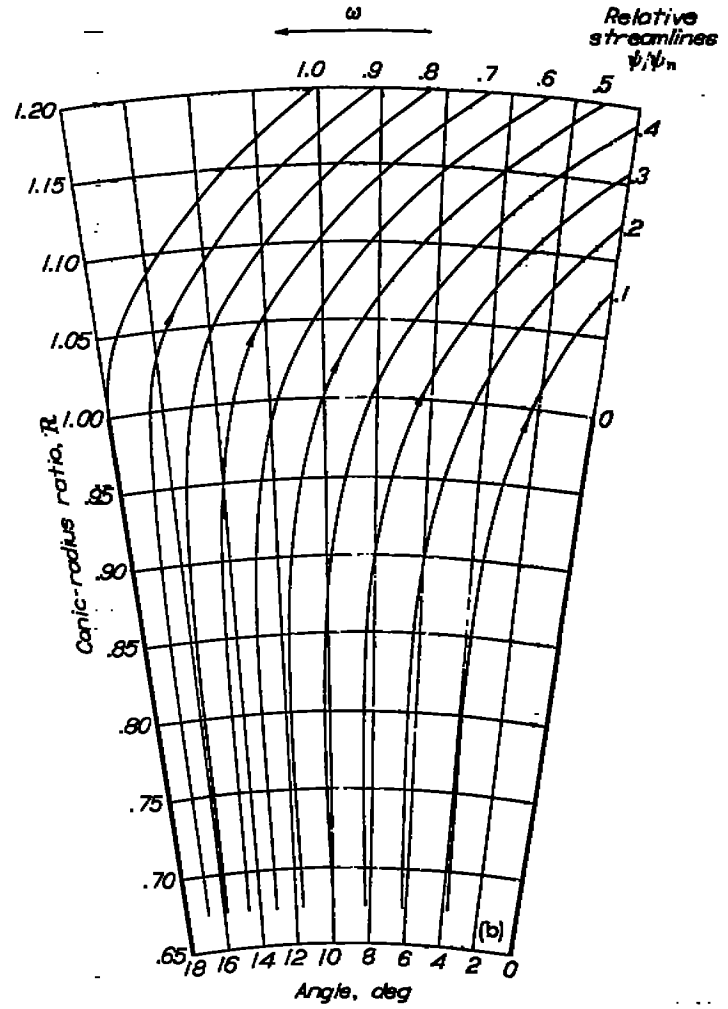

(b) Incompressible-flow example. (Tip Mach number and flow coefficient for the incompressible example are fictitious quantities based on the speed of sound c_0 for compressible example.)

FIGURE 10.—Concluded. Relative streamlines for flow through centrifugal compressor with straight blades. Streamline designation indicates ratio of flow between streamline and positive blade surface (right side of passage) to total flow through passage. Angular blade spacing, 18°; impeller-tip Mach number, 1.5; flow coefficient, 0.5; constant flow area.

From equation (20) the included angle $\Delta\theta$ between blades on the conic flow surface is equal to 18°. The results of the numerical examples are presented in figures 10 to 12. These figures are discussed in the following paragraphs.

Streamlines.—The streamline configurations (relative to the impeller) for the two examples are shown in figure 10. The streamlines are designated in such a manner (ψ/ψ_n) that the value of a streamline indicates the ratio of the flow that lies between the streamline and the positive blade surface to the total flow in the passage. For a given density ratio, the streamline spacing is indicative of the velocities relative to the impeller, with close spacing indicating high velocities and wide spacing indicating low velocities.

In the compressible-flow example (fig. 10(a)), an eddy is attached to the positive blade surface. The fluid in this eddy rotates (relative to the impeller) in the opposite direction to that of the impeller so that the *absolute* motion of the fluid is irrotational. The size of the eddy (for a given impeller) depends on the relative magnitudes of the volume flow rate through the compressor and the impeller-tip speed. If the flow rate is zero through the rotating impeller, the eddy occupies the entire flow passage and as the compressor flow rate increases (for the same impeller-tip speed) the eddy decreases in size until it finally disappears. The flow rate at which the eddy disappears increases as the impeller-tip speed increases. The eddy does not exist in the incompressible-flow example (fig. 10(b)) because, although the weight flow rate is the same for both examples, the *volume* flow rate is higher for the incompressible-flow example as a result of the lower fluid density in the region investigated.

The flow directions in the vaneless diffuser are greatly different for the compressible- and incompressible-flow examples. (Compare figs. 10(a) and 10(b).) This difference results from the higher volume flow rate for the incompressible-flow example. This higher volume flow rate requires higher radial velocities so that for the same tangential velocities the flow directions are different in the two examples. (From considerations of constant moment of momentum in the vaneless diffuser, the tangential velocities should be about the same in both examples because the tangential velocities are about the same at the impeller tip. See subsequent section **Lines of constant pressure ratio.**)

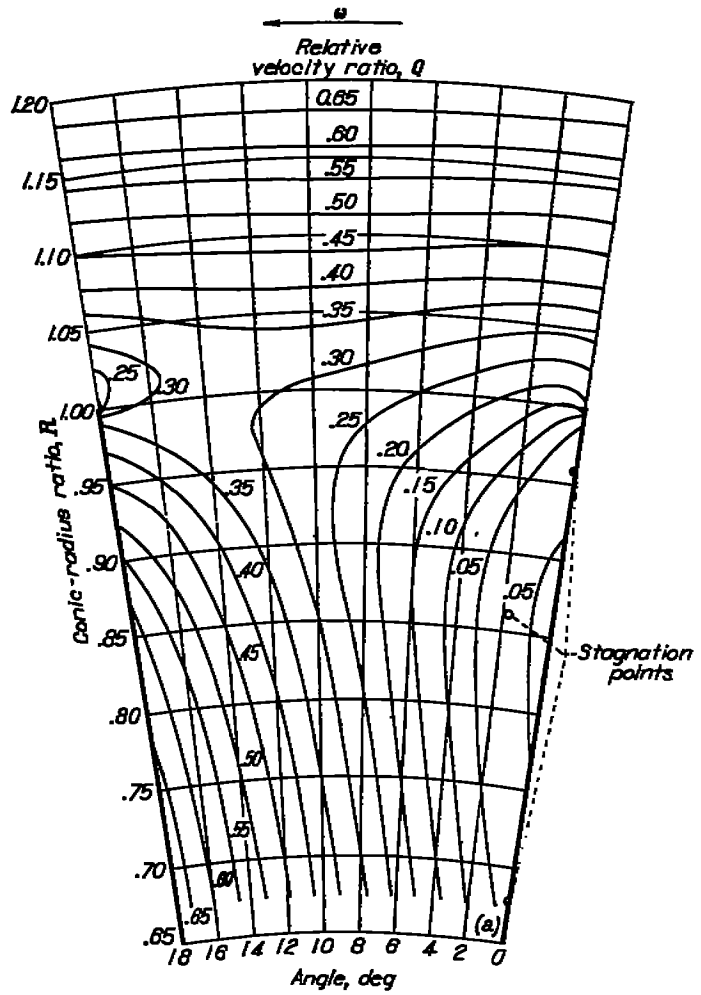

(a) Compressible-flow example.

FIGURE 11.—Lines of constant velocity ratio relative to impeller.

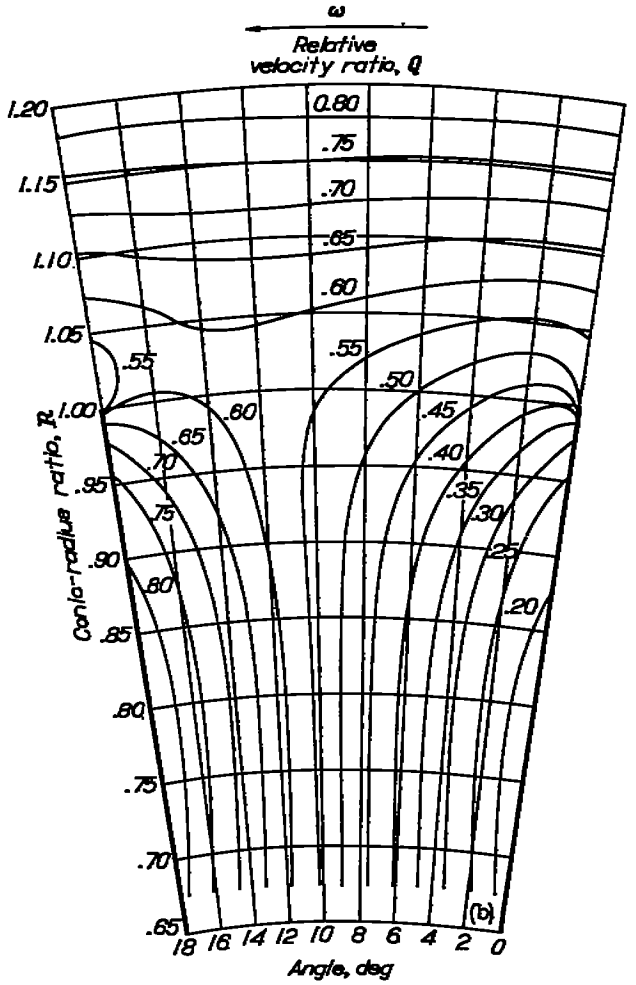

(b) Incompressible-flow example.

FIGURE 11.—Concluded. Lines of constant velocity ratio relative to impeller.

Lines of constant relative velocity ratio.—Lines of constant velocity ratio relative to the impeller are shown for the two examples in figure 11. The constant c_s in the denominator of the velocity ratio is the same for both examples and is equal to the absolute stagnation speed of sound upstream of the impeller for the compressible-flow example. The general characteristics of these plots are similar. The velocities along the negative blade surface are higher than along the positive blade surface except at the tip of the blade where the velocities become equal on both blade surfaces (as required by the Joukowski condition). The maximum velocity occurs on the negative blade surface at a radius ratio well within the impeller and the flow decelerates along the surface of the blade from this point to the blade tip. This deceleration, which becomes rapid near the blade tip, is conducive to boundary-layer separation, which lowers the compressor efficiency. If the boundary-layer wake in the vaneless diffuser is neglected, the velocities become essentially uniform at a radius ratio of about 1.15.

In the compressible example (fig. 11(a)), the velocity ratios are low at the impeller tip because of the high density ratios that result from the high tip speed of the impeller. These velocities would be considerably higher if the effective flow area were reduced by boundary-layer separation, which might be expected in a real compressor.

Lines of constant pressure ratio.—Lines of constant static-pressure ratio (local static pressure divided by absolute stagnation pressure upstream of the blades) are shown for the two examples in figure 12. The general characteristics of these plots are the same. The pressure is higher on the positive blade surface than on the negative blade surface except at the blade tip where the pressures are equal. This difference in pressure accounts for the impeller torque.

The higher pressure ratios in the compressible-flow example than in the incompressible-flow example result from the lower relative velocity ratios in the compressible-flow example and from the fact that for the same amount of work per pound of fluid the pressure ratio is greater for compressible than for incompressible fluids. (That the work per pound of fluid is about the same for both examples at corresponding points is seen from the last term in equation (8). This term is the work per pound of fluid and has about the same values for both examples because the whirl ratio λ is determined principally by the tangential motion of the blades, which is the same in both examples.)

Slip factor.—The impeller slip factor is defined as the ratio of the average absolute tangential velocity of the fluid at the impeller tip to the impeller-tip speed. A method for computing the slip factor from a relaxation solution is outlined in appendix H. The slip factor is 0.899 for the compressible-

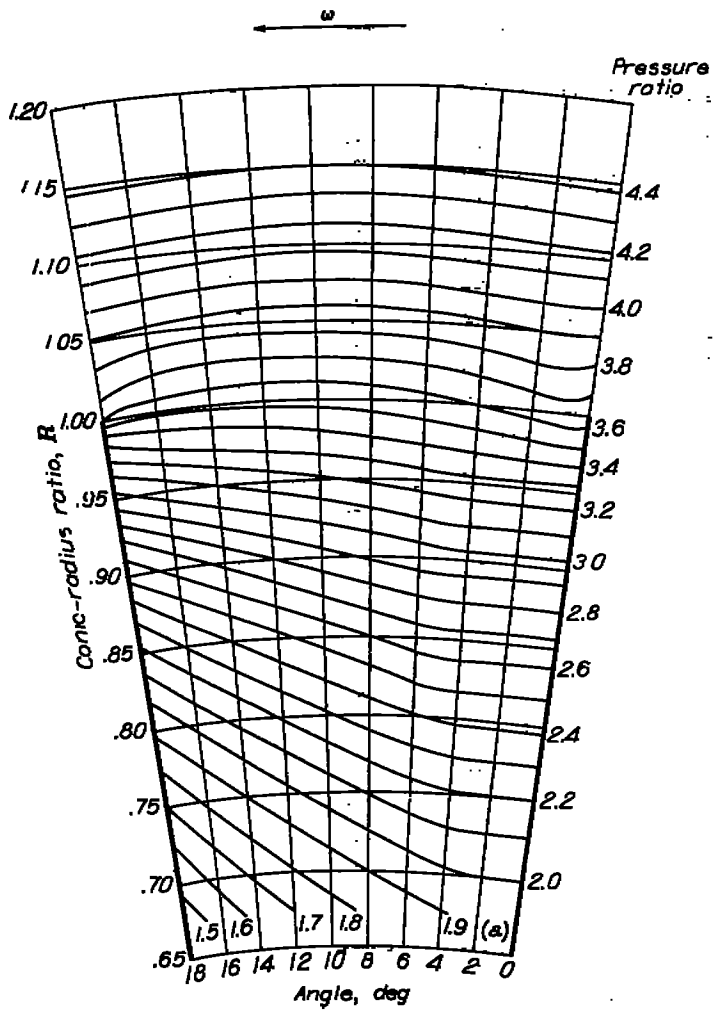

(a) Compressible-flow example.

FIGURE 12.—Lines of constant pressure ratio (local static pressure divided by absolute stagnation pressure upstream of impeller).

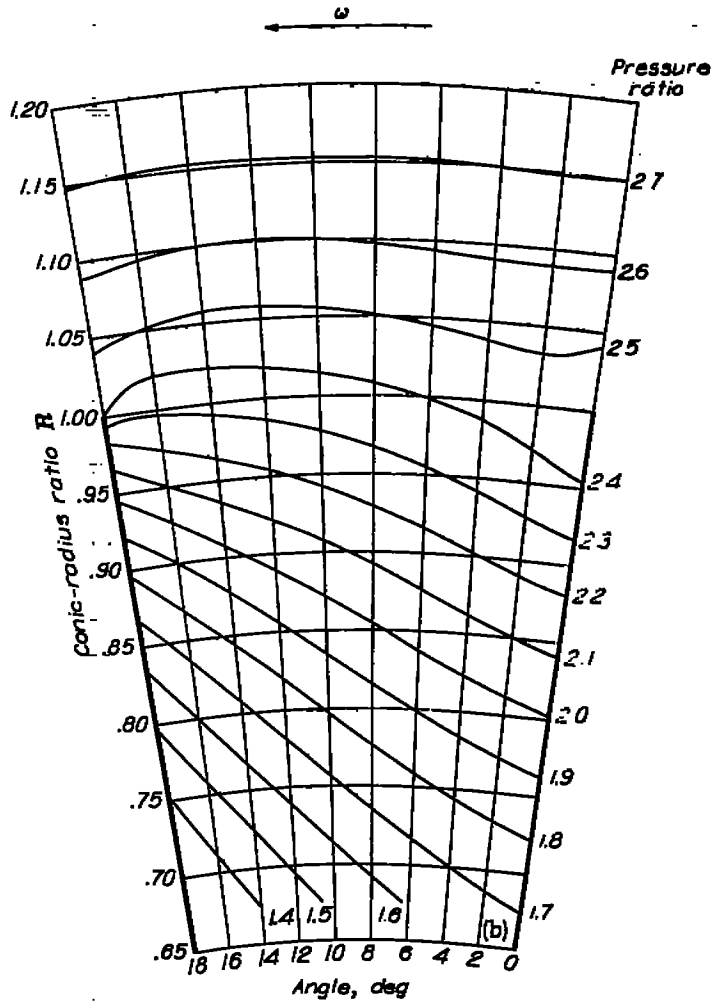

(b) Incompressible-flow example.

FIGURE 12.—Concluded. Lines of constant pressure ratio (local static pressure divided by absolute stagnation pressure upstream of impeller).

flow example and 0.892 for the incompressible example. It is concluded that the slip factors are essentially equal for both examples.

Compressibility effects.—Figure 10 indicates a large compressibility effect upon the streamline configuration in high-speed, rotating, radial- and mixed-flow blade systems. Figures 11 and 12 indicate large compressibility effects upon the magnitudes of the velocity ratios and pressure ratios, but the distribution of these quantities is similar. (For example, the velocities accelerate and decelerate at approximately corresponding positions of the flow field in both examples.) It is concluded that, if the fluid in high-speed, rotating, radial- and mixed-flow turbomachines is compressible, incompressible solutions give poor quantitative results (exception, the slip factor) and, in some respects, poor qualitative results.

SUMMARY OF RESULTS AND CONCLUSIONS

A general method of analysis has been developed for two-dimensional, steady, compressible flow in stators or rotors of radial- and mixed-flow turbomachines with arbitrary blade shapes, arbitrary variations in the passage height, and with conic flow surfaces (surfaces of right circular cones generated by center line of flow passage in axial-radial plane).

The analysis indicates that: (1) The solution obtained for a given turbomachine also applies to certain other (equivalent) turbomachines with a larger or smaller number of like passages (same spacing of the blades on the conic flow surface, same blade-thickness distribution, and so forth) but with different cone angles; (2) for the same number of similar blades, the blade loading is less for mixed-flow than for radial-flow turbomachines; and (3) any solution obtained for an outflow turbomachine with shockless (smooth) entry is also the solution for an inflow turbomachine with shockless entry and with the flow direction and blade rotation (if any) reversed.

Two numerical examples are presented—one for compressible and the other for incompressible flow in a centrifugal compressor with thin, straight blades lying on conic radii (elements). The solutions were obtained in a region of the compressor, including the impeller tip, that was assumed to be unaffected by the inlet configuration of the impeller or by the diffuser vanes (if any). Both examples are for the same impeller (18° included angle between blades on

the conic flow surface) with the same tip speed (equivalent to a tip Mach number of 1.5 for the compressible-flow example), with the same flow rate (flow coefficient, 0.5), and with constant flow area normal to the conic flow surface. The following results were obtained:

(1) In the compressible-flow example, an eddy is attached to the positive blade surface. The fluid in this eddy rotates in the opposite direction to that of the impeller. This eddy does not exist in the incompressible-flow example.

(2) In both examples, the maximum velocity occurs on the negative blade surface at a radius ratio well within the impeller and the flow decelerates along the surface of the blade from this point to the blade tip. This deceleration, which becomes rapid near the blade tip, is conducive to boundary-layer separation, which lowers the compressor efficiency

(3) If the boundary-layer wake in the vaneless portion of the diffuser is neglected, the velocities become essentially uniform at a radius ratio of about 1.15.

(4) The slip factor is 0.899 for the compressible-flow example and 0.892 for the incompressible example. It is concluded that the slip factors are essentially equal for both cases.

(5) If the fluid in high-speed, rotating, radial- and mixed-flow turbomachines is compressible, incompressible solutions give poor quantitative results (exception, the slip factor) and, in some respects, poor qualitative results.

Lewis Flight Propulsion Laboratory,
National Advisory Committee for Aeronautics,
Cleveland, Ohio, *November 1, 1948.*

APPENDIX A

SYMBOLS

The following symbols are used in this report:

a_T	flow area of annulus at tip of blades
B	number of blades (or passages)
b	grid spacing (fig. 3)
c	local speed of sound
c_p	specific heat at constant pressure
e	Cartesian coordinate in transformed ef-plane, equation (C1a)
exp	exponential, $[exp(x)=e^x]$
F	any twice-differentiable function of two variables
f	Cartesian coordinate in transformed ef-plane, equation (C1b)
g	acceleration due to gravity
H	passage-height ratio, h/h_T
h	passage height normal to conic flow surface (fig. 1)
J	mechanical equivalent of heat
M_T	blade-tip Mach number, equation (5)
Q	relative velocity ratio, q/c_o
q	velocity of fluid relative to blades, $\sqrt{u^2+v^2}$
R	conic-radius ratio (coordinate of conic flow surface, $R\theta$-plane) (fig. 2), r/r_T
R	residual
r	conic radius (distance along conic element from apex of cone) (fig. 1)
T	static (stream) temperature
U	relative tangential-velocity ratio, u/c_o (fig. 2)
u	tangential component of q (positive in direction of increasing θ)
V	radial-velocity ratio, v/c_o (fig. 2)
v	radial (along conic element) component of q (positive in direction of increasing radius ratio)
W	total flow rate through turbomachine
w	flow rate between streamlines
α	cone angle (fig. 1)
Γ	dimensionless absolute circulation
γ	ratio of specific heats
$\Delta\theta$	angular blade spacing (included angle between blade camber lines in $R\theta$-plane), equation (20)
$\Delta\psi$	changes in ψ at grid points
η	Cartesian coordinate in transformed $\xi\eta$-plane (corresponds to incompressible stream function in nonrotating $R\theta$-plane with constant passage height, $H=1$), equation (13a)
θ	angle (coordinate of conic flow surface, $R\theta$-plane) (fig. 2)
λ	whirl ratio, equation (9)
ξ	Cartesian coordinate in transformed $\xi\eta$-plane (corresponds to incompressible velocity potential in nonrotating $R\theta$-plane with constant passage height, $H=1$), equation (13a)
ρ	weight density of fluid
ϕ	flow coefficient, equation (24)
ψ	dimensionless, compressible stream function, equations (4a) and (4b)
ω	angular velocity of rotor (in direction of increasing θ)

Subscripts:

A,B,C	grid points defined in figure 7
a,b,c,d	grid points defined in figure 8
D	downstream boundary (boundary in region of uniform flow downstream of blades) (fig. 4)
i	indicates that u_i, v_i, and q_i, obtained from derivatives of $\xi(R,\theta)$ and $\eta(R,\theta)$, correspond to incompressible velocities
n	negative blade surface (blade surface in direction of decreasing θ) (fig. 4(a))
o	absolute stagnation condition in region of uniform flow upstream of blades
p	positive blade surface (blade surface in direction of increasing θ) (fig. 4(a))
T	blade tip (either nose or tail of blade, whichever has larger conic radius)
U	upstream boundary (boundary in region of uniform flow upstream of blades) (fig. 4)
$R,\theta,\xi,\eta,e,$ and f	partial derivatives with respect to these coordinates
RR, $\theta\theta$, $\xi\xi$, $\eta\eta$, $\xi\eta$, ee, and ff	second partial derivatives with respect to these coordinates
1,2,3,4	grid points adjacent to point being considered (fig. 3)

Superscripts:

b'	nonuniform grid spacing defined in figure 7
$\Delta\psi^i$	change in ψ (at any grid point) resulting from $\Delta\psi_D$ required to satisfy Joukowski condition
$\Delta\psi^{ii}$	change in ψ (at any grid point) resulting from $\Delta\psi_D$ equal to unity
ψ^i	adjusted value of ψ (at any grid point) after Joukowski condition is satisfied
ψ_i^*	value of ψ_i (at any point in region of uniform flow upstream of blades) if specified values of λ_U is obtained, equation (F2)

APPENDIX B

TRANSFORMATION OF COORDINATES FROM $R\theta$-PLANE TO $\xi\eta$-PLANE

If the transformation of coordinates from the $R\theta$-plane to the $\xi\eta$-plane is represented by the analytic function

$$\xi(R,\theta)+i\eta(R,\theta)=f[R\ exp\ (i\theta)] \tag{13}$$

where the coordinates ξ and η in the $\xi\eta$-plane correspond to velocity potential lines (ξ=constant) and streamlines (η=constant) in the $R\theta$-plane for incompressible flow past the blades, which for purposes of the transformation are considered to be stationary ($\omega=0$) and to have a constant height ($H=1$), then

$$u_i=-\eta_R=\frac{\xi_\theta}{R} \tag{16a}$$

$$v_i=\frac{\eta_\theta}{R}=\xi_R \tag{16b}$$

Also, if F is any twice-differentiable function of R and θ

$$\left.\begin{aligned}
F_R&=F_\xi\xi_R+F_\eta\eta_R\\
F_{RR}&=F_{\xi\xi}\xi_R^2+2F_{\xi\eta}\xi_R\eta_R+F_{\eta\eta}\eta_R^2+F_\xi\xi_{RR}+F_\eta\eta_{RR}\\
F_\theta&=F_\xi\xi_\theta+F_\eta\eta_\theta\\
F_{\theta\theta}&=F_{\xi\xi}\xi_\theta^2+2F_{\xi\eta}\xi_\theta\eta_\theta+F_{\eta\eta}\eta_\theta^2+F_\xi\xi_{\theta\theta}+F_\eta\eta_{\theta\theta}
\end{aligned}\right\} \tag{B1}$$

From equations (16a), (16b), and (B1), equation (7) becomes

$$\begin{aligned}
2M_TH\frac{\rho}{\rho_e}=&(\psi_{\xi\xi}+\psi_{\eta\eta})(u_i^2+v_i^2)+\psi_\eta\left(\eta_{RR}+\frac{\eta_R}{R}+\frac{\eta_{\theta\theta}}{R^2}\right)+\\
&\psi_\xi\left(\xi_{RR}+\frac{\xi_R}{R}+\frac{\xi_{\theta\theta}}{R^2}\right)-\\
&(\psi_\xi v_i-\psi_\eta u_i)[(\log_e H)_\xi v_i-(\log_e H)_\eta u_i]-\\
&\left[\psi_\xi\left(\log_e\frac{\rho}{\rho_e}\right)_\xi+\psi_\eta\left(\log_e\frac{\rho}{\rho_e}\right)_\eta\right](u_i^2+v_i^2)
\end{aligned}$$

But,

$$q_i^2=u_i^2+v_i^2 \tag{16c}$$

and, because equation (13) is analytic,

$$\xi_{RR}+\frac{\xi_R}{R}+\frac{\xi_{\theta\theta}}{R^2}=0$$

and

$$\eta_{RR}+\frac{\eta_R}{R}+\frac{\eta_{\theta\theta}}{R^2}=0$$

so that equation (7) finally becomes

$$\begin{aligned}
\frac{2M_TH}{q_i^2}\frac{\rho}{\rho_e}=&\psi_{\xi\xi}+\psi_{\eta\eta}-\psi_\xi\left(\log_e\frac{\rho}{\rho_e}\right)_\xi-\psi_\eta\left(\log_e\frac{\rho}{\rho_e}\right)_\eta-\\
&\frac{\psi_\xi v_i-\psi_\eta u_i}{q_i^2}[(\log_e H)_\xi v_i-(\log_e H)_\eta u_i]
\end{aligned} \tag{14}$$

Equation (12) in like manner becomes

$$Q\frac{\rho}{\rho_e}=\frac{q_i}{H}(\psi_\xi^2+\psi_\eta^2)^{1/2} \tag{15}$$

APPENDIX C

$\xi(R,\theta)$ AND $\eta(R,\theta)$ FOR ARBITRARY BLADE SHAPES

The coordinates ξ and η of the transformed $\xi\eta$-plane are functions of R and θ and correspond to the velocity potential $\xi(R,\theta)$ and the stream function $\eta(R,\theta)$ for incompressible flow past blades of arbitrary shape in the physical $R\theta$-plane, which blades are considered, for purposes of the transformation, to be stationary ($\omega=0$) and to have a constant height ($H=1$). In order to determine $\xi(R,\theta)$ and $\eta(R,\theta)$, it is convenient first to transform the blades from the $R\theta$-plane to the ef-plane (e,f Cartesian coordinates). This transformation is given by

$$e+if=\log_e[R\,exp\,(i\theta)]$$

from which

$$e=\log_e R \tag{C1a}$$

$$f=\theta \tag{C1b}$$

Equations (C1a) and (C1b) relate points in the ef-plane to points in the $R\theta$-plane and determine a new blade shape in the ef-plane (fig. 13) that corresponds to the original (arbitrary) blade shape in the $R\theta$-plane (fig. 4(a)). In effect the radial cascade in the $R\theta$-plane is transformed into an axial cascade in the ef-plane.

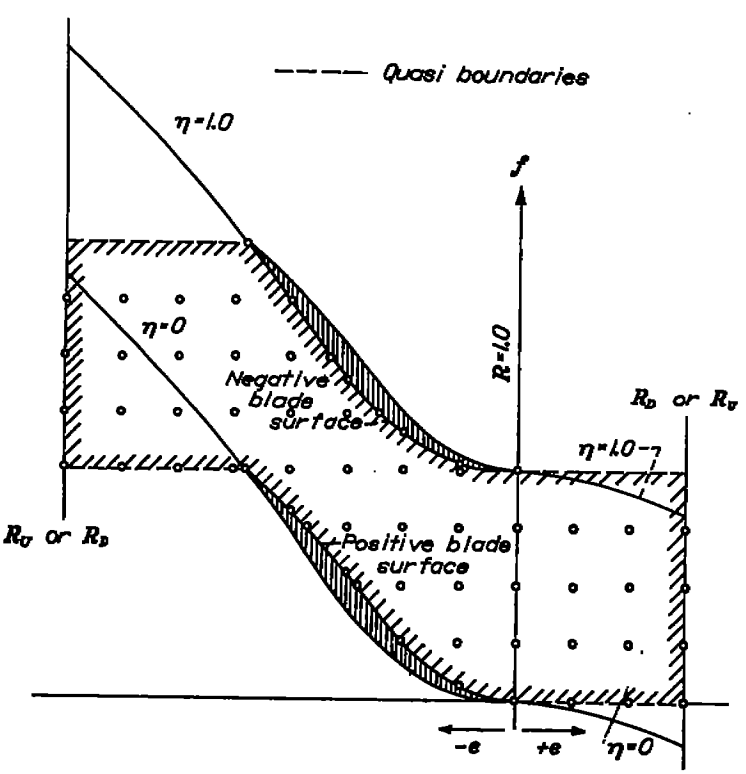

FIGURE 13.—Relaxation grid in ef-plane used to obtain $\eta(e,f)$.

The stream function $\eta(e,f)$ in the ef-plane is determined by the relaxation solution of Laplace's equation

$$\eta_{ee}+\eta_{ff}=0 \tag{C2}$$

for the specified boundary conditions; and the velocity potential $\xi(e,f)$ is obtained from $\eta(e,f)$ by methods discussed in reference 7 (ch. IV). Finally, $\xi(R,\theta)$ and $\eta(R,\theta)$ are determined from $\xi(e,f)$ and $\eta(e,f)$ and from equations (C1a) and (C1b).

In order to solve equation (C2), it is first necessary to determine the boundary conditions. Because the distribution of the variations in η along lines of constant e in the ef-plane is cyclic with a period equal to the blade spacing, the solution of equation (C2) need be obtained only in a region (fig. 13) bounded by the surfaces of two adjacent blades, by lines of constant e that correspond in the $R\theta$-plane to the upstream and downstream boundaries of the compressible-flow field (fig. 4 (a)), and by quasi boundaries extending along lines of constant f from the ends of the blade surfaces to the upstream and downstream boundaries. (Note that these quasi boundaries do not generally, and need not, correspond to the quasi boundaries selected for the compressible-flow field (lines of constant η). See fig. 13.)

After the location of the boundaries has been determined, a grid of equally spaced points is placed inside the boundaries (fig. 13) and this grid is extended to points on the boundaries. The grid points on the blade boundaries generally are unequally spaced from the interior grid points because of the arbitrary shape of the blades. Values of η at points along the quasi boundaries extending from the negative blade surface are directly related to values of η at points along the quasi boundaries extending from the positive blade surface (see related discussion in section ψ **along quasi boundaries extending from positive blade surface**) and, therefore, only the values of η along the quasi boundaries extending from the positive blade surface need be recorded (fig. 13) and relaxed.

The values of η at the grid points on the boundaries are next determined. The boundary values of η at grid points along the blade surface are arbitrarily set equal to 0 along the positive blade surface (fig. 13) and equal to 1.0 along the negative blade surface. The values of η at grid points along the quasi boundaries extending from the positive blade surface are estimated in such a manner that the front and rear stagnation points occur at the intersection of the mean camber line with the surface of the blade at the nose and the tail. The direction of the streamlines is then approximately equal to the direction of the blade camber line at the ends of the blade. This direction is defined in the ef-plane by

$$\tan\beta=\frac{df}{de} \tag{C3}$$

But along a streamline, $d\eta$ equals zero so that

$$d\eta=0=\eta_e de+\eta_f df$$

$$\frac{df}{de}=-\frac{\eta_e}{\eta_f} \tag{C4}$$

Also, if uniform flow is assumed upstream and downstream of the blades, then from equation (C1b) and the specified boundary conditions

$$\eta_f=\frac{\Delta\eta}{\Delta f}=\frac{1}{\Delta\theta} \tag{C5}$$

Therefore, from equations (C3), (C4), and (C5),

$$\eta_e=-\frac{\tan\beta}{\Delta\theta} \tag{C6}$$

This variation in η with e determines estimated values of η at grid points along the quasi boundaries extending from the positive blade surface and in particular this variation determines the values of η at the intersections of these quasi boundaries with the upstream and downstream boundaries (fig. 13). Along these upstream and downstream boundaries, the values of η increase uniformly (steady-flow condition) in the positive direction of f at a unit rate per blade spacing.

After the boundary values of η have been determined, values of η are estimated at the interior grid points. These estimated values are generally in error and must be corrected by relaxation methods in which equation (C2) is used in finite-difference form to compute and to relax the residuals. In addition, the values of η along the quasi boundaries extending from the positive blade surface were estimated values and must therefore be relaxed. After the solution for the distribution of η has been obtained, the condition that the stagnation points occur at the nose and the tail of the blades is checked (by methods similar to those in appendix E) and, if not satisfied, the values of η at the grid points along the upstream and downstream boundaries are adjusted (by methods similar to those outlined in appendix E).

The function $\eta(e,f)$ is now known and $\xi(e,f)$ can be determined from $\eta(e,f)$ by methods given in reference 7 (ch. IV).

The functions $\eta(R,\theta)$ and $\xi(R,\theta)$ are obtained directly from $\eta(e,f)$ and $\xi(e,f)$ and from equations (C1a) and (C1b). Also, from equations (16) and (C1), the coefficients u_t and v_t in equations (18) and (19) become

$$u_t=-\eta_R=-\frac{\eta_e}{R} \tag{C7a}$$

$$v_t=\frac{\eta_\theta}{R}=\frac{\eta_f}{R} \tag{C7b}$$

The relaxation solution of equations (11), (14), and (15) in the transformed $\xi\eta$-plane requires less time than the solution of equations (7), (11), and (12) in the physical $R\theta$-plane, because blades with arbitrary shape in the physical plane become straight and parallel in the transformed plane, which results in simpler finite-difference forms for equations (14) and (15). The transformation of coordinates to the $\xi\eta$-plane is time-consuming, however, so that, if a solution for only one set of operating conditions is desired, it would probably be faster to solve equations (7), (11), and (12) in the ef-plane where, although the finite-difference equations must contain coefficients to account for the unequal grid spacing along the irregular boundaries, the transformation of coordinates is given directly by equations (C1a) and (C1b). If, however, solutions for a number of different operating conditions for the same blade configuration are desired, then the transformation of coordinates outlined in this appendix is desirable, because the same transformation applies to all sets of operating conditions for the same blade configuration.

APPENDIX D

ESTIMATED VALUES OF ψ AT GRID POINTS ALONG QUASI BOUNDARIES EXTENDING FROM POSITIVE BLADE SURFACE IN $\xi\eta$-PLANE

Estimated values of the stream function ψ at grid points along the quasi boundaries extending from the positive blade surface in the $\xi\eta$-plane can be obtained by assuming, as a first approximation, that the flow conditions upstream and downstream of the blades in the $R\theta$-plane are uniform, that is, the flow conditions are a function of R only. From the conservation of absolute moment of momentum (whirl) upstream and downstream of the blades

$$\lambda=R(RM_T\mp U)=\text{constant} \tag{D1}$$

so that equation (4b) becomes

$$\psi_R=\frac{\rho}{\rho_o}H\left(RM_T-\frac{\lambda}{R}\right) \tag{D2}$$

In addition, because the flow is considered uniform

$$\psi_\theta=\text{constant}=\frac{\psi_n}{\Delta\theta} \tag{D3}$$

The variation in ψ along the quasi boundaries in the $\xi\eta$-plane (fig. 6) is then given by

$$\psi_\xi=\psi_R R_\xi+\psi_\theta\theta_\xi$$

which, from equations (D2) and (D3) becomes

$$\psi_\xi=\frac{\rho}{\rho_o}H\left(RM_T-\frac{\lambda}{R}\right)R_\xi+\frac{\psi_n}{\Delta\theta}\theta_\xi \tag{D4}$$

where R_ξ and θ_ξ are obtained from equations (13a) or appendix C. Equation (D4) gives the estimated variation in ψ along the quasi boundaries extending from the positive blade surface in the $\xi\eta$-plane.

In order to integrate equation (D4), it is necessary to know the variation in density with ξ. The density ratio is given by equation (11)

$$\frac{\rho}{\rho_o}=\left\{1+\frac{\gamma-1}{2}\left[(RM_T)^2-Q^2-2M_T\lambda_U\right]\right\}^{\frac{1}{\gamma-1}} \tag{11}$$

where, from equation (3a),

$$Q^2=U^2+V^2 \tag{D5}$$

But, from continuity considerations assuming uniform flow,

$$V^2=\left(\frac{\phi}{\frac{\rho}{\rho_o}HR}\right)^2 \tag{D6}$$

so that, from equations (D1), (D5), and (D6),

$$Q^2=\left(\frac{\lambda}{R}-RM_T\right)^2+\left(\frac{\phi}{\frac{\rho}{\rho_o}HR}\right)^2$$

and equation (11) becomes

$$\frac{\rho}{\rho_o}=\left\{1+\frac{\gamma-1}{2}\left[2M_T(\lambda-\lambda_U)-\left(\frac{\lambda}{R}\right)^2-\left(\frac{\phi}{\frac{\rho}{\rho_o}HR}\right)^2\right]\right\}^{\frac{1}{\gamma-1}} \tag{D7}$$

Because R is a known function of ξ and η (equation (13a) or appendix C), the system of equations (D4) and (D7) can be solved by numerical methods to obtain the value of ψ at grid points along the quasi boundaries extending from the positive blade surface in the $\xi\eta$-plane (fig. 6).

The values of ψ depend on the value of λ. Upstream of the blades λ has the specified value λ_U. Downstream of the blades λ has the value λ_D, which for a given blade shape and operating condition, is determined by the Joukowski condition. As a result of the Joukowski condition, the average flow direction at the exit from the blades is approximately equal to the blade-exit angle (determined by the mean camber line). An average value of U, required in equation (9) to compute an estimated value of λ_D, can therefore be obtained from this angle (adjusted as experience indicates) and from the average value of V given by continuity considerations (equation (D6)).

APPENDIX E

METHOD OF ADJUSTING VALUES OF ψ ALONG DOWNSTREAM BOUNDARY TO SATISFY JOUKOWSKI CONDITION

The Joukowski condition requires the rear stagnation point to occur at the blade tail, or, in case of infinitely thin blades or blades with cusped tails, the flow must be tangent to the blade surfaces at the tail. (If the blade tail is somewhat rounded, the stagnation point is considered to occur at the intersection of the mean camber line with the tail surface of the blade.) In the $\xi\eta$-plane (fig. 6), this rear stagnation point occurs at the tail of the thin, straight blade. (See appendix C.) This condition generally is not satisfied by the initial relaxation solution for ψ in the $\xi\eta$-plane, because for this solution the values of ψ along the downstream boundary (ψ_D) were obtained from the estimated variation in ψ along the quasi boundaries (appendix D). In order to satisfy the Joukowski condition, the values of ψ at the grid points along the downstream boundary (ψ_D) must all be changed the same required amount ($\Delta\psi_D$). This change in ψ_D (denoted by $\Delta\psi_D$) results in changes in ψ (denoted by $\Delta\psi$) at each of the interior grid points and at the grid points along the quasi boundaries. The manner in which the values of ψ are changed by the change in ψ_D must satisfy the difference equation (18). Therefore,

$$(\psi_1+\Delta\psi_1)+(\psi_2+\Delta\psi_2)+(\psi_3+\Delta\psi_3)+(\psi_4+\Delta\psi_4)-4(\psi+\Delta\psi)-$$
$$\frac{(\psi_1+\Delta\psi_1)-(\psi_3+\Delta\psi_3)}{4}\left(\log_e\frac{\rho_1}{\rho_e}-\log_e\frac{\rho_3}{\rho_e}\right)-$$
$$\frac{(\psi_2+\Delta\psi_2)-(\psi_4+\Delta\psi_4)}{4}\left(\log_e\frac{\rho_2}{\rho_e}-\log_e\frac{\rho_4}{\rho_e}\right)-$$
$$\frac{1}{4q_t^2}\{[(\psi_1+\Delta\psi_1)-(\psi_3+\Delta\psi_3)]v_t-[(\psi_2+\Delta\psi_2)-(\psi_4+\Delta\psi_4)]u_t\}\times$$
$$\{(\log_e H_1-\log_e H_3)v_t-(\log_e H_2-\log_e H_4)u_t\}-$$
$$\frac{2M_THb^2}{q_t^2}\frac{\rho}{\rho_e}=\mathrm{R} \qquad \text{(E1)}$$

where the change in density ratio resulting from $\Delta\psi$ is considered negligible. Subtracting equation (18) with R equal to zero (which condition has been satisfied by the initial relaxation) from equation (E1) results in

$$\Delta\psi_1+\Delta\psi_2+\Delta\psi_3+\Delta\psi_4-4\Delta\psi-\frac{\Delta\psi_1-\Delta\psi_3}{4}\left(\log_e\frac{\rho_1}{\rho_e}-\log_e\frac{\rho_3}{\rho_e}\right)-$$
$$\frac{\Delta\psi_2-\Delta\psi_4}{4}\left(\log_e\frac{\rho_2}{\rho_e}-\log_e\frac{\rho_4}{\rho_e}\right)-\frac{1}{4q_t^2}[(\Delta\psi_1-\Delta\psi_3)v_t-(\Delta\psi_2-\Delta\psi_4)u_t]\times$$
$$[(\log_e H_1-\log_e H_3)v_t-(\log_e H_2-\log_e H_4)u_t]=\mathrm{R} \qquad \text{(E1a)}$$

Each of the last three terms on the left side of equaltion (E1a) consists of the product of two quantities that approach zero as the grid spacing b approaches zero. For the small grid spacing used in relaxation solutions, these terms are therefore of secondary importance and may be neglected so that

$$\Delta\psi_1+\Delta\psi_2+\Delta\psi_3+\Delta\psi_4-4\Delta\psi=\mathrm{R} \qquad \text{(E1b)}$$

The solution of equation (E1b) determines $\Delta\psi$ at every grid point for a specified value of $\Delta\psi_D$. Because of the linearity of equation (E1b), the solution for any specified value of $\Delta\psi_D$ is equal to the solution for $\Delta\psi_D=1.0$ multiplied by the specified value of $\Delta\psi_D$. That is, $\Delta\psi$ (at any grid point) resulting from a specified value of $\Delta\psi_D$ is equal to $\Delta\psi$ (at the grid point) resulting for $\Delta\psi_D=1.0$ multiplied by the specified value of $\Delta\psi_D$.

The procedure for the solution of equation (E1b) is the same as for equation (18). The boundary values of ψ along the blade surfaces and along the upstream boundary (fig. 6) are not changed so that $\Delta\psi$ must equal zero along these boundaries. The value of $\Delta\psi$ along the downstream boundary (fig. 6) is set equal to unity.

The magnitude of $\Delta\psi_D$ required to satisfy the Joukowski condition can now be determined as follows: If the rear stagnation point occurs at the blade tail (Joukowski condition), then the extrapolated value for ψ at the grid point on the blade tail of the positive blade surface obtained from the values of ψ at succeeding points along the quasi boundary starting at the blade tail must equal zero. The extrapolated value of ψ at the blade tail using a third-degree polynomial and the first four points along the quasi boundary is given by

$$\psi_{tail}=4\psi_a-6\psi_b+4\psi_c-\psi_d$$

where the subscripts a, b, c, and d refer to the grid points along the quasi boundary in figure 8. If ψ_{tail} equals zero,

$$0=4\psi_a^t-6\psi_b^t+4\psi_c^t-\psi_d^t \qquad \text{(E2)}$$

where ψ^t signifies values of ψ after the Joukowski condition is satisfied. But,

$$\psi^t=\psi+\Delta\psi^t \qquad \text{(E3)}$$

where ψ is the stream function obtained by the initial relaxation and $\Delta\psi^t$ is the change in ψ that results when the Joukowski condition is satisfied. Also, from the first part of this appendix,

$$\Delta\psi^t=\Delta\psi_D\Delta\psi^{tt} \qquad \text{(E4)}$$

where $\Delta\psi^{tt}$ is the change in ψ (at any grid point) resulting from a unit change in ψ_D ($\Delta\psi_D=1.0$) and $\Delta\psi_D$ is the change in ψ_D required to satisfy the Joukowski condition. Therefore, from equations (E2), (E3), and (E4))

$$\Delta\psi_D=\frac{-4\psi_a+6\psi_b-4\psi_c+\psi_d}{4\Delta\psi_a^{tt}-6\Delta\psi_b^{tt}+4\Delta\psi_c^{tt}-\Delta\psi_d^{tt}} \qquad \text{(E5)}$$

Equation (E5) determines the change in ψ_D required to satisfy the Joukowski condition. The changes in ψ at all other grid points are obtained by multiplying $\Delta\psi^{tt}$ at each grid point by $\Delta\psi_D$. Because the solution for $\Delta\psi^{tt}$ is approximate, the resulting values of ψ^t must usually be relaxed to eliminate small residuals computed by equation (18).

APPENDIX F

METHOD OF ADJUSTING VALUES OF ψ ALONG UPSTREAM BOUNDARY TO OBTAIN SPECIFIED WHIRL RATIO λ_U

In general, the specified whirl ratio upstream of the blades λ_U is not obtained by the initial relaxation solution, because for this solution the values of ψ along the upstream boundary (ψ_U) were obtained from the estimated variation in ψ along the quasi boundaries (appendix D). In order to obtain the specified value of λ_U, the values of ψ at the grid points along the upstream boundary (ψ_U) must all be changed the same required amount ($\Delta\psi_U$). This change in ψ_U (denoted by $\Delta\psi_U$) results in changes in ψ (denoted by $\Delta\psi$) at each of the interior grid points and at the grid points along the quasi boundaries. The effect of $\Delta\psi_U$ on the values of $\Delta\psi$ is determined in the same manner as the effect of $\Delta\psi_D$ on the values of $\Delta\psi$ (appendix E).

The magnitude of $\Delta\psi_U$ required to obtain the specified value of λ_U can now be determined as follows: Near the upstream boundary in the region where flow conditions are essentially uniform, the whirl ratio λ is constant and equal to λ_U. In this region equation (9) gives

$$\lambda_U = R(RM_T + U) \tag{9}$$

where U is related to the variation in ψ by equation (4b)

$$\psi_R = -\frac{\rho}{\rho_e} UH \tag{4b}$$

But,

$$\psi_R = \psi_\xi \xi_R + \psi_\eta \eta_R \tag{F1}$$

where for uniform flow conditions

$$\psi_\eta = \psi_n$$

so that, from equations (16a) and (16b), equation (F1) becomes

$$\psi_R = \psi_\xi v_\xi - \psi_n u_\xi \tag{F1a}$$

Therefore, from equations (F1a), (4b), and (9)

$$\psi_\xi^* = \frac{1}{v_\xi}\left[u_\xi \psi_n - \frac{\rho}{\rho_e} H\left(\frac{\lambda_U}{R} - RM_T\right)\right] \tag{F2}$$

where ψ_ξ^* is the value of ψ_ξ at any point in the region of uniform flow upstream of the blades if the specified whirl ratio λ_U is obtained and where ρ/ρ_e is considered to be given by the initial relaxation solution. (In general, equation (F2) is evaluated at the upstream boundary where, assuming conditions are uniform, ψ_ξ is constant.)

If ψ_ξ is obtained by the initial relaxation solution at the point being considered in the region of uniform flow, the $\Delta\psi_U$ required to obtain the value of ψ_ξ^* (equation (F2)) corresponding to the specified value of λ_U is given by

$$\Delta\psi_U = \frac{\psi_\xi^* - \psi_\xi}{(\Delta\psi)_\xi} \tag{F3}$$

where $(\Delta\psi)_\xi$ is the variation in $\Delta\psi$ with ξ, at the point being considered, for a unit change in ψ_U. Equation (F3) determines the change in ψ_U required to obtain the specified value of λ_U.

The resulting changes in ψ at the interior grid points and at the grid points along the quasi boundaries are determined from $\Delta\psi_U$ in the same manner as the changes in ψ were determined from $\Delta\psi_D$ in appendix E. It should be noted that the correction for λ_U will affect the Joukowski condition, and vice versa. For high-solidity blades, however, the effect of $\Delta\psi_D$ on λ_U and the effect of $\Delta\psi_U$ on the Joukowski condition is generally small and can be neglected.

APPENDIX G

SIMPLIFIED ANALYSIS FOR ROTORS WITH STRAIGHT BLADES ALONG CONIC RADII

The relaxation methods used in this report are lengthy. It would therefore be advantageous to have a quicker, although less accurate, means of estimating the flow conditions. In this appendix, a simplified analysis is developed for rotors with straight blades along conic radii.

Velocity-ratio distribution.—This simplified analysis is based on the assumption that for rotors with straight blades along conic radii the tangential component of the velocity ratio relative to the blades is zero within the rotor. Equation (6) therefore reduces to

$$V_\theta=2RM_T \tag{G1}$$

which, when integrated, becomes

$$V=V_p+2RM_T\theta \tag{G2}$$

where the subscript p refers to the positive blade surface at which surface the angle θ is considered zero. Equation (G2) gives the distribution of the radial component of the velocity ratio across the passage at constant values of R. The constant of integration V_p is determined at each value of R from considerations given in the next paragraph.

Stream-function distribution.—From continuity

$$dw=\rho vhrd\theta$$

or

$$\frac{dw}{\rho_s c_s h_T r_T}=\frac{\rho}{\rho_s}VHRd\theta \tag{G3}$$

The density ratio is given by equation (11) with Q equal to V (because U is assumed equal to zero) and V is given by equation (G2) so that equation (G3) becomes

$$d\psi=HR\left\{1+\frac{\gamma-1}{2}[(RM_T)^2-(V_p+2RM_T\theta)^2-2M_T\lambda_U]\right\}^{\frac{1}{\gamma-1}}(V_p+2RM_T\theta)d\theta \tag{G4}$$

where the left side of equation (G4) was obtained from equation (21). Equation (G4) is integrated from the positive blade surface where ψ and θ are considered equal to zero so that

$$\psi=\frac{H}{2\gamma M_T}\left[\left\{1+\frac{\gamma-1}{2}[(RM_T)^2-V_p^2-2M_T\lambda_U]\right\}^{\frac{\gamma}{\gamma-1}}-\left\{1+\frac{\gamma-1}{2}[(RM_T)^2-(V_p+2RM_T\theta)^2-2M_T\lambda_U]\right\}^{\frac{\gamma}{\gamma-1}}\right] \tag{G5}$$

Equation (G5) gives the distribution of ψ across the passage at constant values of R. The velocity ratio V_p varies with R and is obtained from equation (G5) for the condition

$$\psi=\psi_n$$

when

$$\theta=\theta_n$$

If the fluid is incompressible, the distribution of ψ becomes

$$\psi=HR(V_p\theta+RM_T\theta^2)$$

Numerical example.—The simplified analysis has been applied to the compressible-flow example in this report and the results are compared with those of the relaxation solution. The velocity ratio V_p along the positive blade surface has been computed from equation (G5) and the results are compared in figure 14 with the relaxation solution. The negative values of V_p occur where the eddy (fig. 10(a)) is attached to the blade. The agreement between the relaxation solution and the simplified solution is satisfactory up to a radius ratio of about 0.80. For radius ratios greater than 0.80, the agreement is unsatisfactory because the assumption that U and its derivative are negligible is no longer valid.

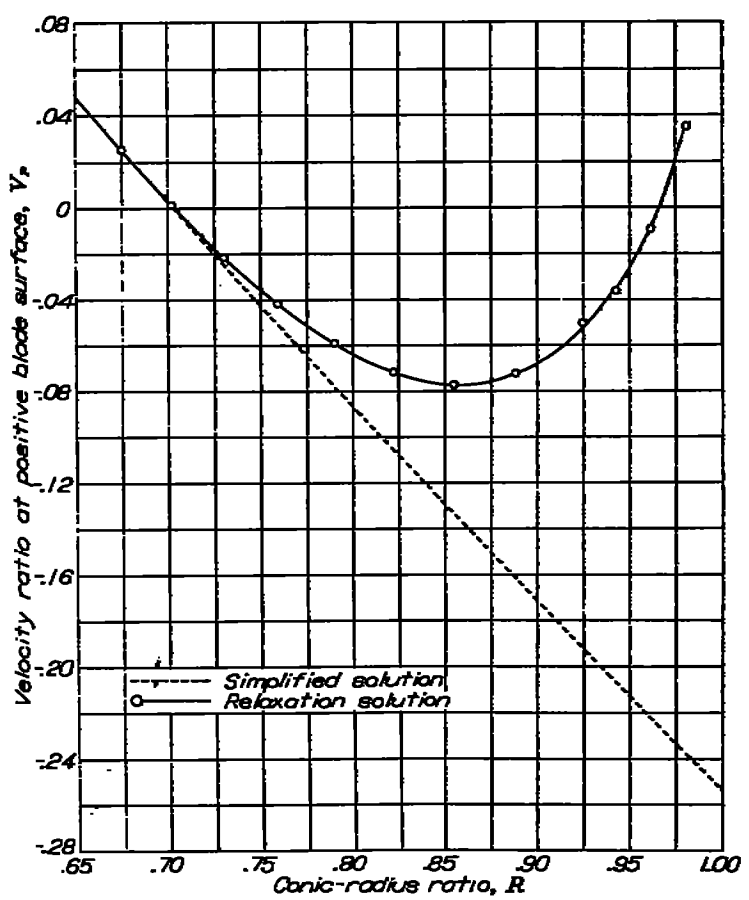

FIGURE 14.—Comparison of velocity ratio along positive blade surface for simplified and relaxation solutions.

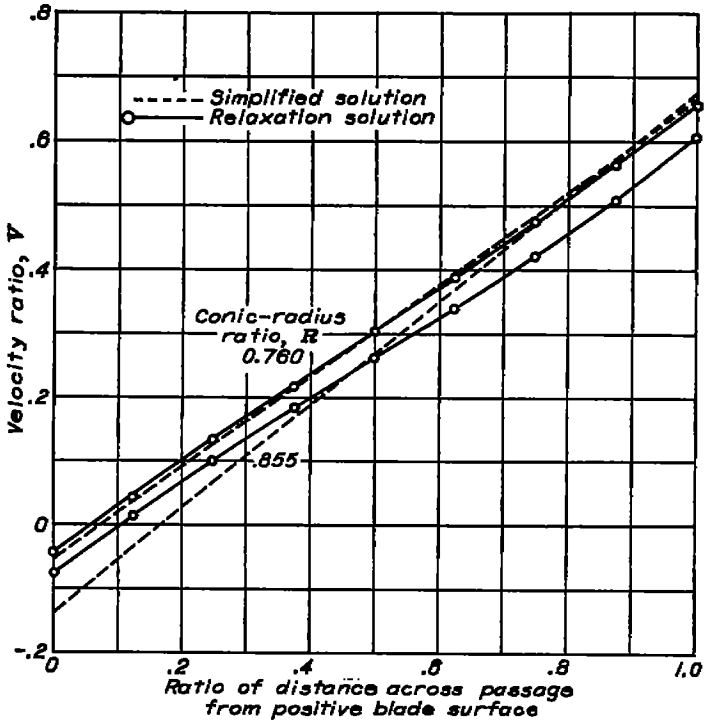

FIGURE 15.—Comparison of velocity distribution across passage for simplified and relaxation solutions.

The velocity-ratio distributions across the passage at radius ratios of 0.760 and 0.855 have been computed from equation (G2) using values of V_s obtained from equation (G5) and the results are compared in figure 15 with the relaxation solution. At the 0.760 radius ratio, the velocity distribution is nearly the same for both solutions, but at the 0.855 radius ratio the simplified solution has begun to deviate from the more rigorous relaxation solution.

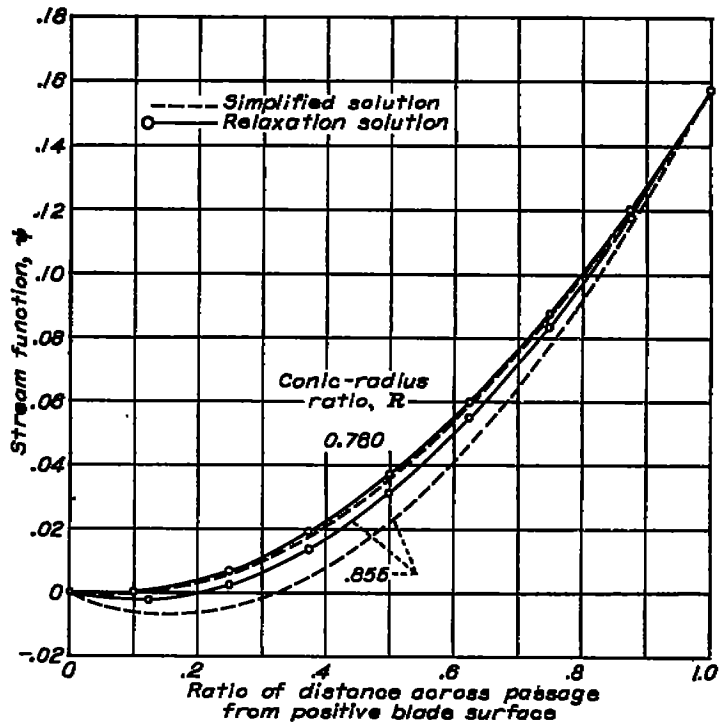

FIGURE 16.—Comparison of stream-function distribution across passage for simplified and relaxation solutions.

The stream-function distributions across the passage at radius ratios of 0.760 and 0.855 have been computed from equation (G5) and the results are compared in figure 16 with the relaxation solution. At a radius ratio of 0.760 the stream-function distribution is nearly the same for both solutions, but at 0.855 the simplified solution has begun to deviate appreciably from the relaxation solution.

APPENDIX H

PROCEDURE FOR COMPUTING IMPELLER SLIP FACTOR

The impeller slip factor for centrifugal compressors is defined as the ratio of the average absolute tangential velocity of the air at the impeller tip to the tip speed of the impeller

$$\text{Slip factor}=\frac{\left(\omega r_T \sin\frac{\alpha}{2}+u\right)_{av}}{\omega r_T \sin\frac{\alpha}{2}}=1+\frac{U_{av}}{M_T} \qquad \text{(H1)}$$

The average value of the tangential-velocity ratio relative to the impeller at the impeller tip is obtained from

$$u_{av}=\frac{\int_{\theta_p}^{\theta_n} u\rho v h_T r_T\, d\theta}{\int_{\theta_p}^{\theta_n} \rho v h_T r_T\, d\theta}$$

or

$$U_{av}=\frac{\rho_e \mathcal{L}_e h_T r_T}{\frac{W}{B}}\int_{\theta_p}^{\theta_n} UV\frac{\rho}{\rho_e}\, d\theta$$

which, from equation (22), becomes

$$U_{av}=\frac{1}{\psi_n}\int_{\theta_p}^{\theta_n} UV\frac{\rho}{\rho_e}\, d\theta \qquad \text{(H2)}$$

Equation (H2) gives a weighted average value of U. This weighted average is also equal to the unweighted average

$$\frac{1}{\theta_n-\theta_p}\int_{\theta_p}^{\theta_n} U d\theta$$

This fact can be shown from considerations of the conservation of moment of momentum in the vaneless diffuser, which is based upon the weighted average of U and from considerations of constant absolute circulation in the diffuser, which is based upon the unweighted average of U.

Combining equations (H1) and (H2) results in the following expression for the slip factor:

$$\text{Slip factor}=1+\frac{1}{\psi_n M_T}\int_{\theta_p}^{\theta_n} UV\frac{\rho}{\rho_e}\, d\theta \qquad \text{(H3)}$$

The value of the integrand is obtained from the relaxation solution.

REFERENCES

1. Stodola, A.: Steam and Gas Turbines. Vol. II. McGraw-Hill Book Co., Inc., 6th ed., 1927, pp. 998–1006, 1255–1260.
2. Sörensen, E.: Potential Flow through Centrifugal Pumps and Turbines. NACA TM 973, 1941.
3. Betz, A., and Flügge-Lotz, I.: Design of Centrifugal Impeller Blades. NACA TM 902, 1939.
4. Bollay, William: The Theory of Flow through Centrifugal Pumps. Theodore von Kármán Anniversary Vol., Contributions to Appl. Mech. and Related Subjects, C. I. T., May 11, 1941, pp. 278–284.
5. Concordia, C., and Carter, G. K.: D-C Network-Analyzer Determination of Fluid-Flow Pattern in a Centrifugal Impeller. Jour. Appl. Mech., vol. 14, no. 2, June 1947, pp. A113–A118.
6. Southwell, R. V.: Relaxation Methods in Engineering Science. Clarendon Press (Oxford), 1940.
7. Southwell, R. V.: Relaxation Methods in Theoretical Physics. Clarendon Press (Oxford), 1946.
8. Emmons, Howard W.: The Numerical Solution of Compressible Fluid Flow Problems. NACA TN 932, 1944.
9. NACA Subcommittee on Compressors: Standard Procedures for Rating and Testing Multistage Axial-Flow Compressors. NACA TN 1138, 1946.
10. Emmons, Howard W.: The Numerical Solution of Partial Differential Equations. Quarterly Appl. Math., vol. II, no. 3, Oct. 1944, pp. 173–195.